Rigorous physicochemical framework for metal ion binding by aqueous nanoparticulate humic substances : implications for speciation modeling by the NICA-Donnan and WHAM codes

Rigorous Physicochemical Framework for Metal Ion Binding by Aqueous Nanoparticulate Humic Substances: Implications for Speciation Modelling by the NICA-Donnan and WHAM Codes

Journal:	*Environmental Science & Technology*
Manuscript ID	es-2019-00624h.R2
Manuscript Type:	Critical Review
Date Submitted by the Author:	n/a
Complete List of Authors:	Town, Raewyn; Universiteit Antwerpen, Systemic Physiological and Ecotoxicological Research (SPHERE) Van Leeuwen, Herman; & Colloid Science, Lab.for Physical Chemistry Duval, Jerome; CNRS, Laboratoire Interdisciplinaire des Environnements Continentaux CNRS UMR7360

Rigorous Physicochemical Framework for Metal Ion Binding by Aqueous Nanoparticulate Humic Substances: Implications for Speciation Modelling by the NICA-Donnan and WHAM Codes

Raewyn M. Town[1,2]*, Herman P. van Leeuwen[2], Jérôme F. L. Duval[3],

[1] Systemic Physiological and Ecotoxicological Research (SPHERE), Department of Biology, University of Antwerp, Groenenborgerlaan 171, 2020 Antwerp, Belgium. Tlf: +32-3-2653535, email: raewyn.town@uantwerpen.be

[2] Physical Chemistry and Soft Matter, Wageningen University & Research, Stippeneng 4, 6708 WE Wageningen, The Netherlands.

[3] CNRS – Université de Lorraine, Laboratoire Interdisciplinaire des Environnements Continentaux (LIEC), UMR 7360 CNRS, 15 avenue du Charmois, 54500 Vandoeuvre-les-Nancy, France.

ABSTRACT

Latest knowledge on the reactivity of charged nanoparticulate complexants towards aqueous metal ions is discussed in mechanistic detail. We present a rigorous generic description of electrostatic and chemical contributions to metal ion binding by nanoparticulate complexants, and their dependence on particle size, particle type (*i.e.* reactive sites distributed within the particle body or confined to the surface), ionic strength of the aqueous medium, and the nature of the metal ion. For the example case of soft environmental particles such as fulvic and humic acids, practical strategies are delineated for determining intraparticulate metal ion speciation, and for evaluating intrinsic chemical binding affinities and heterogeneity. The results are compared with those obtained by popular codes for equilibrium speciation modelling (namely NICA-Donnan and WHAM). Physicochemical analysis of the discrepancies generated by these codes reveals the *a priori* hypotheses adopted therein and the inappropriateness of some of their key parameters. The significance of the characteristic timescales governing the formation and dissociation rates of metal-nanoparticle complexes in defining the relaxation properties and the complete equilibration of the metal/nanoparticulate complex dispersion is described. The dynamic features of nanoparticulate complexes are also discussed in the context of predictions of the labilities and bioavailabilities of the metal species.

1. INTRODUCTION

Nanoparticles (NPs), both natural and engineered ones, are ubiquitous in natural waters and encompass a wide range of physical and chemical properties. In terms of particle types, distinction can be made between:

(i) soft particles, which are permeable to water and ions, and incorporate reactive sites distributed within the volume of the particle body, *e.g.* humic substances, polysaccharides, dendrimers, and

(ii) hard impermeable particles with reactive sites confined to the particle surface, *e.g.* metals and metal oxides, silica, and graphene, and

(iii) core-shell particles comprising an impermeable core and a permeable coating, *e.g.* iron oxides particles coated with natural organic matter, or various functionalized engineered NPs (Fig. 1).

NPs that are dispersed in aquatic systems generally carry a net charge, often negative, and thus have the potential to electrostatically impact on the chemical speciation dynamics and ensuing bioavailability of trace metal cations (M for short). A defining characteristic of NPs is that their structural charges and reactive sites are physically confined to the particle body and/or surface, where conditions, *e.g.* pH, concentration of reactant ions, *etc*., may be very different from those prevailing in the bulk aqueous medium.[1-3] A proper interpretation of metal ion binding by dispersed NPs is bound to take these features into explicit account. Recent years have witnessed significant advances in conceptual understanding of the thermodynamic and kinetic features of metal ion interaction with NPs. The developed interpretation methodologies integrate the physical and chemical features of the local nano- to micro-environments where the actual complexation process takes place, *e.g.* the influence of the particle's electric field and the governing intraparticulate concentrations of complexing sites and reactant metal ions. Notably, the approach enables delineation of the Poisson-Boltzmann-based electrostatics and the covalent chemical contributions to metal ion association, together with the ensuing characterisation of the *intraparticulate* metal speciation. Such detail is essential in the context of dynamic metal speciation analysis and bioavailability. The theoretical framework provides good agreement with experimental data, for both well-defined engineered NPs, *e.g.* functionalized latex particles,[4,5] and heterogeneous natural soft NPs, *e.g.* humic and fulvic acids.[6-9]

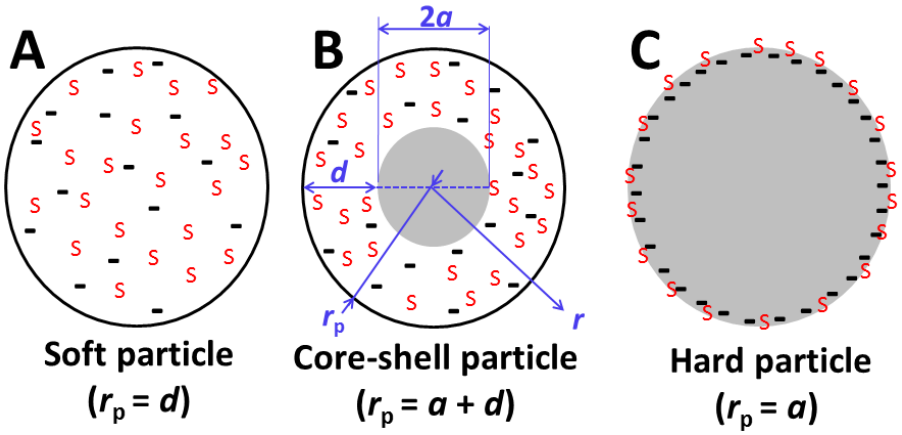

Figure 1. Schematic representation of (A) soft, (B) core-shell, and (C) hard nanoparticles. The particle radius, r_p, is equal to the sum of the thickness of the soft shell, d, and the radius of the impermeable core, a. Soft NPs have $a = 0$, and hard NPs have $d = 0$.

Humic substances (HS for short) are natural heterogeneous complexants that exhibit characteristics typical of soft charged NPs.[10] Their effective radii in aqueous dispersion ranges from the order of 1 nm to 100 nm depending on their origin and aggregation state. The structural details of the particles are not rigorously known, and in aqueous dispersions individual HS particles may represent an ensemble of several entities.[11-13] Indeed, analysis of HS by soft electron ionisation Fourier transform ion cyclotron resonance mass spectrometry (FT-ICR-MS) identifies a large number of small fragments, albeit that their identity is typically not unambiguous,[14] and the technique is inherently biased towards detection of lighter (fragment) ions.[15] Whilst spectrometrically identified fragments of HS have been used as inputs for molecular dynamic simulations of HS properties,[16] the information is inherently not representative of particles in aqueous dispersion. In present context, the average physicochemical properties of HS in aqueous dispersion are the relevant descriptors.

Over the years, equilibrium modelling codes have been developed to compute metal ion speciation in the presence of HS, e.g. the widely used NICA-Donnan and WHAM codes.[17-21] These two models involve very different types of constituent parameters for both the electrostatic and chemical contributions to metal ion binding, and are based on distinctly different starting hypotheses (Table 1). At the time of their first formulation in the late 1980s/early 1990s,[22-25,] both approaches represented a pragmatic means to tackle the challenge of describing metal binding by HS. In agreement with acid-base titration data, both models consider two major types of HS complexing sites, nominally carboxyl and phenolic functional groups. For the electrostatics, both models assume a Donnan-type electrostatic field, albeit within different spatial domains (see Section 3). For the intrinsic chemical binding, WHAM employs a constrained set of discrete binding sites, whereas NICA-Donnan assumes a continuous distribution of binding affinities. Given their very different approaches, the finding that both NICA-Donnan and WHAM predict similar concentrations of free metal ions in the presence of dissolved organic matter underscores their empirical foundations.[26,27]

Table 1. Key components of the NICA-Donnan and WHAM models for description of metal ion association with humic substances

Model	Electrostatic binding	Chemical binding and heterogeneity
NICA-Donnan	• Donnan partitioning defined by an empirically co-fitted Donnan volume, V_D, and Donnan potential, ψ_D, unconstrained by the particle size, thus potentially including the extraparticulate zone. • V_D is dependent on solution ionic strength, I, according to: $\log V_D = b(1-\log I)-1$, where b is an empirical factor.	• Continuous, bimodal Sips distribution of binding sites. • Model parameters include affinity constants for proton and metal ion binding with each of the two types of binding sites (nominally carboxylic and phenolic), width of the distribution of the two types of binding sites, generic heterogeneity parameters for each type of binding site, and ion-specific non-ideality parameters for each metal ion which are implemented as scaling factors and reflect an ill-defined combination of the degree of correlation between the proton and metal ion affinity distribution, the dentism, and the reaction stoichiometry.[17-19,28] • Proton heterogeneity and metal specific heterogeneity parameters are partly correlated.[29] • Multidentate binding is allowed only between sites of the same type.[30] • Stability constants for metal ion binding derived from fitting of the model to published datasets.
WHAM VII	• Extraparticulate Donnan partitioning in a shell with thickness equal to the Debye screening length in the bulk solution. • Additional empirical "electrostatic correction factor", with no defined spatial zone. • An empirical constant to adjust the volume of the extraparticulate double layer at low charge to prevent the counterion concentration therein from being lower than that in the bulk solution.	• Mixture of discrete binding sites. • Model parameters include the density of nominal carboxylic and phenolic sites, a central proton affinity for each type of site which together with a spread term is used to generate a total of 4 carboxyl and 4 phenolic sites of different proton affinity and abundance, certain fractions of which may bind metal ions via mono-, bi-, and tri-dentate configurations (calculated probabilistically); allowed combinations yield a total of 50 different metal binding configurations.[21] • The intrinsic metal binding affinity is the same for all 4 carboxyl sites, and for all 4 phenolic sites. An additional factor that represents interactions with N and S functional groups is used to generate strong metal binding sites. Stability constants for metal binding are derived from fitting of the model to published datasets in combination with linear free energy relationships (LFERs). In absence of experimental data, LFERs are used to generate binding constants from conventional equilibrium constants for simple ligands.[20,21,31,32]

Recent advances in understanding of the reactivity of NPs[1-5] has established robust insights into metal cation association with HS.[6-9] Herein we scrutinise the current understanding of the generic physicochemical reactivity of NPs with focus on both the thermodynamic and the dynamic features of their association and dissociation reactions with metal ions. The concepts are generically applicable to all types of NPs (Fig. 1), regardless of whether they are natural or engineered.[33] For present purposes we focus on HS to illustrate the

concepts for environmentally relevant soft, charged NPs, and critically assess the robustness and consistency of the electrostatic and chemical descriptors in comparison with the outcomes of the aforementioned equilibrium speciation codes. Practical examples are further presented to illustrate the underlying concepts.

2. SMEARED-OUT *versus* INTRAPARTICULATE CONCENTRATIONS

At the outset, it is fundamental to distinguish between smeared-out concentrations, *i.e.* conventional concentrations for chemical species averaged over the entire volume of the nanoparticle dispersion, versus the local intraparticulate species concentrations. Conventionally,[4,34] metal ion binding is described in terms of smeared-out concentrations, *i.e.*:

$$\overline{K}_{\mathrm{app}} = \bar{c}_{\mathrm{M,b}} / \left[c_{\mathrm{M}}^{*} (\bar{c}_{\mathrm{S,t}} - \bar{c}_{\mathrm{M,b}}) \right] \quad (1)$$

where $\overline{K}_{\mathrm{app}}$ is the apparent stability constant of the metal-particle associates, $\bar{c}_{\mathrm{M,b}}$ is the smeared-out total concentration of all forms of M associated with the nanoparticulate complexant, c_{M}^{*} is the concentration of free metal ion in the bulk solution, and $\bar{c}_{\mathrm{S,t}}$ is the smeared-out total concentration of the NP metal ion binding sites. The overbar notation signifies that $\overline{K}_{\mathrm{app}}$ represents a weighted average of the stabilities over all associated forms of M with the complexant. Early studies on nanoparticles described their complexation behavior in terms of smeared-out concentrations,[4,35] which fails to properly represent the local nature of the complexation processes and the key importance of interfacial particle electrostatics. For example, use of the terminology "bound M" to collectively refer to all species of M associated with a soft NP is deceptive because it includes the intraparticulate free M and the merely electrostatically associated metal forms located within *and* in the close vicinity of the NP body. Meaningful descriptors for the thermodynamic and kinetic features of metal cation association/dissociation with nanoparticulate complexants are bound to account for the fact that the reactive complexant sites are spatially confined to the particulate body and/or surface, inside the position-dependent electric field of the charged NP.[3] Speciation codes generally apply concentrations of chemical species as smeared-out values with the consequence that the significance of the results is not transparent in terms of the relevant species and the local intraparticulate physicochemical conditions involved. Throughout the following text we shall take care to discriminate between local, intraparticulate concentrations of a given species *i*, denoted by c_i, and corresponding smeared-out concentrations, denoted by $\bar{c}_i$; bulk free ion concentrations are denoted by c_i^{*}.

3. ELECTROSTATIC FEATURES OF CHARGED NANOPARTICLES

The electric field of soft and charged aquatic nanoparticles contributes to the extent to which counterions associate with the particle body. This feature is evidenced by the effect of ionic strength on *e.g.* proton titration curves.[36] Thus mechanistic understanding of metal ion binding to soft and charged aquatic nanoparticles necessarily calls for a critical assessment of the NPs electrostatic features as a function of relevant medium parameters, such as salinity and pH. The characteristic electrostatic parameter of the bulk electrolyte solution is the Debye length, κ^{-1}, which represents the characteristic thickness of the region surrounding the charged

NP within which the concentrations of counter- and coions differ from their bulk solution values. The magnitude of κ is given by:

$$\kappa^2 = e^2 \sum_i z_i^2 c_i^* N_{\mathrm{Av}} / \varepsilon\varepsilon_0 k_{\mathrm{B}} T \quad (2)$$

with e the elementary charge, c_i^* the bulk concentration of ions of type i with valency z_i, N_{Av} the Avogadro number, $\varepsilon\varepsilon_0$ the dielectric permittivity of the electrolyte solution, k_{B} the Boltzmann constant, and T the temperature. For the sake of simplicity, we assume below that the charged groups located within the volume or at the surface of the NPs (case of soft and hard NPs, respectively) are also the reactive, metal binding groups, and that these groups are homogeneously distributed (over the particle volume and surface, respectively). For completeness, we note that the presence of merely charged groups inside the NP is straightforwardly invoked in the electrostatic characterization of the system.[37,38] The local concentration of charges generates a corresponding particle electric field, the quantitative nature of which depends on such parameters as particle size, charge density, and particle permeability to ions. Different types of nanoparticulate potential profiles are distinguished based on the relative magnitude of the separation distance ℓ_{C} between charged groups carried by the NP as compared to the Debye screening length. Strictly speaking, the relevant screening length for soft NP bodies is the *intraparticulate* one, κ_{p}^{-1} (see below and Section 3.2 for further discussion of κ^{-1} *cf.* κ_{p}^{-1}).[39] For transparency, we proceed with consideration of the high charge density case,[2] *i.e.* the situation in which $\kappa_{\mathrm{p}}\ell_{\mathrm{C}} << 1$, implying that the individual charges cooperate in a joint particle electric field.

Evidently a proper interpretation of metal ion association with charged NPs requires knowledge on the particle electric field distribution, *e.g.* at the simplest level, merely to establish whether a Donnan representation is applicable or not. Techniques based on electrokinetic phenomena, *e.g.* electrophoresis, are useful tools to probe the charge density characteristics of dispersed NPs as well as their electric double layers at the particle/medium interface.[40] The basis concept of a zeta-potential developed for hard (ion-impermeable) particles,[41] is not applicable to soft NPs due to the absence of a discrete slip plane at the interphase they form with the electrolytic medium (see ref 42 and references cited therein). Retrieving soft particle electrostatic properties from electrokinetic measurements requires resorting to formalisms that explicitly account for electroosmotic flow penetration within the particle body (the so-called particle hydrodynamic softness).[39,42-45] A model of particular interest, originally proposed by Ohshima,[39] is applicable to soft particles with size that legitimates Donnan electric representation under the given electrolyte concentration conditions, *i.e.* $\kappa r_{\mathrm{p}} >> 1$ (see details in Supporting Information). Classically, the electrophoretic mobility of soft particles is measured over a large range of 1-1 electrolyte concentrations c_1^*, typically 1 to 100 mM, and Ohshima's model is adopted to capture the dependence of μ on c_1^*, from which particle hydrodynamic softness and charge density together with the Donnan potential can be evaluated. Below a given threshold value of c_1^*, the inequality $\kappa r_{\mathrm{p}} >> 1$ is violated, and Ohshima's model no longer holds.[42-46] Proper description of the experimental data in this transition range of c_1^* values then requires resorting to sophisticated numerical evaluation of the complete set of electro-

hydrodynamic equations, as extensively detailed elsewhere.[42-46] All in all, measurements of particle electrophoretic mobility *versus* medium salt concentration, and analysis thereof with adequate formalisms, offer a useful and practical route to evaluate the correctness of Donnan electrostatic representation and, if applicable, the sign, magnitude and pH-dependence of the Donnan potential and corresponding (volume) charge density of soft particles. The attempts to interpret metal ion binding to soft HS NPs on the basis of NICA-Donnan or WHAM models hardly refer to - nor integrate - independent particle electrokinetic measurements for validating or constraining the required or derived particle electrostatic details. In contrast, example studies for HS based on the generic Poisson-Boltzmann framework, as adopted for modelling particle electrokinetic properties, can be found in literature.[6,10,47,48]

The profile and magnitude of the particle electric field influences the rate and extent to which oppositely charged ions associate with the particle *via* electrostatic interactions, and its spatial distribution defines the zone over which such interactions are operational. Specifically, the particle electric field has an influence on (i) the rate of diffusion of metal ions towards the particle body, which is modified by a coefficient for conductive diffusion, $\overline{f}_{\mathrm{el}}$,[49] and on (ii) the extent to which ions partition between the bulk solution and the particle interface/body, as described by the pertaining Boltzmann partitioning factors, $\overline{f}_{\mathrm{B}}$, and, where relevant, by a counterion condensation factor, $\overline{f}_{\mathrm{C}}$.[7,8] In the first instance, we consider the effect of the particle electric field on the *extent* of ion association with charged NPs at equilibrium. The impact of the particle electric field on the *rate* of formation/dissociation of metal complexes is discussed in section 5.

When a dispersion of charged particles is equilibrated with ions in aqueous electrolyte media, there is an accumulation of counterions in the extraparticulate zone of the NP body, and, in the case of core-shell and soft NPs, this accumulation adds to that in the intraparticulate volume. The relative contributions of extraparticulate and intraparticulate accumulations depend on particle type, size and charge density, as well as on the nature of the background electrolyte (*e.g.* 1-1 *vs*. 2-1) and on the ionic strength of the bulk aqueous medium. The characteristic features of the various types of electrostatic interactions are described in the following sections.

3.1. Mean-field Poisson-Boltzmann description of NP electrostatic features

The mean-field Poisson-Boltzmann (PB) approach has been used to describe the extraparticulate and intraparticulate distributions of the electrostatic potential and corresponding electric field. The PB framework has some well-documented limitations, especially under conditions where solution ionic strength well exceeds *ca.* 200 mM, notably it does not account for ion size, nor counterion condensation.[50,51] Nevertheless, the electrostatic features of small soft NPs with a radius, r_{p}, similar in size to the Debye screening length in the bulk medium, κ^{-1}, have been fairly well described by PB counterion accumulation in both the intra- and extra-particulate volume.[6,52] For small soft particles with $\kappa_{\mathrm{p}} r_{\mathrm{p}}$ of the order unity, the extraparticulate accumulation of metal cations can become significant relative to the total amount of M associated with the particle. The extent to which the particle electric field develops into the surrounding medium depends on the type of background electrolyte (*e.g.* 1-1 *vs*. 2-1) and the ionic strength of the aqueous medium. Conventionally, the

particle field and potential distribution are modelled on the basis of the density of *structural* charges carried by the NP. Recent work has identified the importance of considering the particle's field/potential profiles in completely relaxed (*i.e.* fully equilibrated) ion partition configuration with the electrolyte in the medium.[6,53] In the case of small NPs ($r_p \approx \kappa^{-1}$), such consideration picks up differences in the thickness of the extraparticulate zone where counterion accumulation is significant.In the case of large and highly charged soft particles whose radius largely exceeds the characteristic Debye length, the PB framework alone is insufficient to explain the influence of the electric field on ion association: such particles necessarily couple their Donnan partitioning in the particle body with intraparticulate counterion condensation in the highly charged electric double layer (DL) at the particle/medium interface.[7-9] Depending on particle size, local net charge density within the DL, and solution ionic strength, the dominant process may be Donnan partitioning or counterion condensation, or both may be operational. The leading features are discussed below.

3.2. Donnan partitioning

In the case of environmental soft HS NPs, the majority of the literature, as well as the NICA-Donnan and WHAM models, assume that the electrostatic association between counterions and the NPs involves Donnan partitioning. It is important to realise however that the electrostatic Donnan representation for the electric potential distribution within, and in the direct vicinity of a given charged particle, corresponds to a particular limit of the more generic Poisson-Boltzmann equation.[54,55] Indeed such a representation is strictly applicable under conditions where the particle radius, r_p, is much larger than the thickness of the *intraparticulate* Debye layer, κ_p^{-1}, *and* where the charge density is sufficiently high so that $\kappa_p \ell_C << 1$. We note that the defining expression for κ_p, $\kappa_p = \kappa\{\cosh(F\psi_D / RT)\}^{1/2}$,[39,55] includes the Donnan potential term ψ_D. In the literature it is more common to see the condition for applicability of a Donnan phase in a highly charged body as being r_p much greater than the Debye screening length in the *bulk* electrolyte solution, κ^{-1}. This latter condition is more severe (because $\kappa_p^{-1} \le \kappa^{-1}$), but has the advantage to depend only on the ionic strength of the medium and not on the Donnan potential itself. When the conditions $\kappa_p r_p >> 1$ and $\kappa_p \ell_C << 1$ are both met, the Donnan potential difference, ψ_D, is established between the bulk of the soft NP body and the bulk aqueous solution. For a symmetrical *z*:*z* electrolyte with concentration c_1^*, ψ_D is defined by the following expression:[39,55]

$$\psi_D = \frac{RT}{zF}\operatorname{asinh}\left(\frac{\rho_p}{2zFc_1^*}\right) \tag{3}$$

where ρ_p is the volume density of structural charges randomly distributed on the backbone of the soft NP body. An implicit expression is further available to compute ψ_D in 2-1 electrolyte.[8,56] Ions of type *i* and valency z_i partition between the Donnan phase (where their concentration is $c_{i,D}$) and the bulk aqueous electrolyte solution (where their concentration is c_i^*) according to a Boltzmann type partitioning factor, $\overline{f}_B$, defined by:[57]

$$\overline{f}_B = \frac{c_{i,D}}{c_i^*} = \exp\left(\frac{-z_i F\psi_D}{RT}\right) \tag{4}$$

By definition, the Donnan volume, V_D, comprises an *intraparticulate* zone which cannot be larger than the volume of the particle body, V_p. In this Donnan volume, for highly charged NPs, the charges originating from counter-ions exactly compensate the structural charges carried by the NP therein. The contribution of the coions in setting this charge balance depends on the magnitude of the charge density carried by the NPs. In turn, a Donnan volume features a constant electrostatic (Donnan) potential, a zero electric field and a zero *net* charge density. These fundamental physicochemical conditions are violated by the WHAM and NICA-Donnan speciation codes in their modelling of humic complexes as outlined in Section 1. Furthermore, both models erroneously consider that the electrostatic contribution to ion association can be described purely by Donnan partitioning, irrespective of particle size, and ignore the presence of a highly charged interfacial double layer,[58,59] without which a Donnan regime would not exist. The WHAM model further assumes that Donnan partitioning is exclusively *extraparticulate*, *i.e.* V_D (per particle) is given by:[20]

$$V_D = \frac{4\pi}{3}\left[(r_p + \kappa^{-1})^3 - r_p^3\right] \quad (5)$$

The situation expressed by eq 5 is physicochemically meaningless: the extraparticulate double layer carries a given charge density (originating from dissimilar distributions of background electrolyte co- and counter-ions) *but* no structural NP charges are present therein. The formulation then amounts to effectively ignoring the complete double layer features from the soft particle centre to the outer electrolyte solution, which implies that there cannot be a properly defined bulk Donnan particle. WHAM invokes an empirical "electrostatic correction factor" to calculate the local concentration of counterions in the vicinity of the reactive sites, given by $\exp(-2wzZ)$, where z is the charge on the binding ion, Z is the charge on the humic molecule (eq g^{-1}), and w = P×log$I$, where P is an empirical factor and I is the ionic strength of the bulk solution (mol dm^{-3}).[20] The spatial scale over which the electrostatic correction applies is not made explicit, and its connection to the concentration of counterions in V_D is not transparent.

The NICA-Donnan model also ignores fundamental principles for the existence of a Donnan phase: the V_D adjusted to 'model' metal-binding isotherms is allowed to be even *greater* than V_p.[28] A Donnan volume that exceeds the physical particle volume comes to violation of the Poisson-Boltzmann equation because *stricto sensu* V_D corresponds to the volume in which the overall net charge density of the particle is zero (for the high charge density Donnan case this overall charge predominantly stems from structural NP charges and counterions). The NICA-Donnan model obtains V_D by *co-fitting* of V_D and ψ_D to protolytic titrations. This strategy is necessarily redundant because the Donnan volume, if applicable, can be estimated from knowledge of the Poisson-Boltzmann-derived potential distribution at the NP/medium interphase, *i.e.* from the decrease of the potential from Donnan to NP surface potential values (see details in Section 3.4). The NICA-Donnan approach results in a V_D that is apparently dependent on the ionic strength of the aqueous medium according to its empirical double-logarithmic expression for V_D:[60]

$$\log V_D = b(1 - \log I) - 1 \quad (6)$$

where V_D has units of $dm^3\ kg^{-1}$ HS, b is a fitting parameter and I is the ionic strength of the aqueous medium. In order to invoke an ionic strength dependence of V_D it is necessary to establish (i) the ionic strength-dependent swelling/contraction of the particle and/or (ii) the ionic strength-dependence of the spatial zone of the particle body where the potential equals ψ_D and the remaining part of the particle (the intraparticulate double layer) where the potential drops from ψ_D to the NP surface potential. Upon increasing r_p at fixed solution ionic strength (or conversely), V_D should asymptotically increase towards V_p, but can never exceed the particle dimensions. In its implementation, the NICA-Donnan model does not verify the aforementioned factors. Furthermore, the physicochemical reasonableness of other electrostatic descriptors in the NICA-Donnan model are questionable. For example, the ionic strength dependence of V_D, as expressed by eq 6, is in conflict with experimental data which show that the HA particle size is practically independent of ionic strength in the range from 0 to several hundreds of mM.[61-63] In general, the NICA-Donnan electrostatic descriptors for humic substances appear to overestimate the magnitudes of contributing factors, *i.e.* significant Boltzmann factors are obtained at low degrees of proton dissociation,[59,60] and the generic values for ψ_D are significantly more negative than those experimentally determined for HS by electrokinetic measurements.[64] For example, at pH 4 and I = 10 mM, a ψ_D value of *ca*. -100 mV is computed for FA using the generic NICA-Donnan parameters,[64] as compared to the average potential in the particle body of -36 mV determined by electrokinetic techniques.[35] Finally, it is worth mentioning that the V_D, ψ_D couple determined by the NICA-Donnan model is sensitive to how the fitting is implemented,[64] which underscores the empirical nature of the approach. We return to this issue in subsequent sections.

3.3. Counterion condensation

When the structural charge density of a polyion exceeds a certain threshold value, the counterions tend to condense in the close vicinity of the charges so as to reduce the net local charge density. Specifically, counterion condensation is operative when the charge separation distance is less than the Bjerrum length, *i.e.* the length for which the electrostatic attraction energy equals k_BT (where k_B is the Boltzmann constant).[65] The theory for purely electrostatic condensation was first developed by Manning for linear polyelectrolytes,[65,66] and the phenomenon has since been established for spherical geometries, *e.g.* dendrimers,[67-69] and core-shell NPs with 3D structural charge in the soft shell.[70] Condensed ions may retain some degree of hydration and a finite mobility within the spatial zone of condensation.[71]

For the case of a linear polyelectrolyte, in the absence of background electrolyte, the limiting condensation law for the number of associated z-valent counterions per structural monovalent charge, θ_z, is given by:[71]

$$\theta_z = (z\xi - 1) / z^2\xi \quad (7)$$

where ξ is the dimensionless structural charge density parameter:[65]

$$\xi = e^2 / \varepsilon k_B T \ell_C \quad (8)$$

with e the elementary charge and $e^2 / \varepsilon k_B T$ the Bjerrum length with ε the relative dielectric permittivity of the solution. For the case of condensation of a divalent cation by a linear polyanion, in 1-1 background

electrolyte (well in excess over the smeared-out concentration of anionic charges), under conditions where charge compensation by the divalent cations M^{2+} is much greater than that by the monovalent electrolyte cations, Manning derived the analytical expression:[71]

$$\log(\theta_2 / c^*_{M^{2+}}) = \log(V_c / 2.718) - 4\xi(1-2\theta_2)\log(1-\exp(-\kappa\ell_c)) \quad (9)$$

where $c^*_{M^{2+}}$ is the bulk concentration of free M^{2+} and V_c denotes the condensation volume per mole of structural charge (m^3 mol^{-1}) for associated counterions.

In the case of soft particles which are of sufficient size and charge density to meet the criteria $\kappa_p r_p >> 1$ and $\kappa_p \ell_C << 1$ (see Section 3.2.), condensation will occur within the negatively charged intraparticulate DL (thickness ℓ_{DL}, volume V_{DL}) at the particle/medium interface and not in the remaining volume of the particle. It has been observed that electrostatic condensation in a volume distribution of structural charges already occurs at greater charge separation distances as compared to the 1D case detailed by Manning.[7] Although analytical expressions, analogous to eqs 7-9, for condensation in well-defined 3D geometries are not yet available, the relevant parameters (ℓ_{DL}, condensation limit $\overline{f}_C$) can be obtained from experimental data on binding of electrostatically associating ions such as Ca^{2+} (see Section 3.5).[8,9]

3.4. Counterion condensation-Donnan (CCD) model

For the case of large, highly charged HA particles, which meet the criterion for applicability of Donnan electrostatics over the practical range of ionic strengths, evidence for condensation-type behavior has been reported in the binding of divalent counterions that predominantly associate by electrostatic interactions, *e.g.* Ca^{2+} and Ba^{2+}.[72] Furthermore, the extent to which Ca^{2+} associates with HA is orders of magnitude greater than that predicted on the basis of Donnan partitioning alone.[7] These observations led to development of the two state counterion condensation-Donnan (CCD) model for purely electrostatic association with the charged NP.[8,9] The CCD model combines Donnan partitioning within the bulk zone of the soft NP (volume V_D) with counterion condensation in the intraparticulate part of the electric double layer (volume V_{DL}) at the particle/medium interface. The dimensions are constrained by the size of the particle, *i.e.* $V_p = V_D + V_{DL}$. For the large HA considered herein, the volume fraction ratio of the double layer and Donnan volumes is much less than unity, *i.e.* $\kappa_p r_p >> 1$. Under these conditions the extent of Boltzmann accumulation of M^{2+} in the extraparticulate double layer is negligible relative to the total amount of M associated with the particle. Where relevant, the excess M in the extraparticulate zone can be obtained from the diffuse double layer potential profile.[49] The two-state electrostatic CCD model is shown schematically in Fig. 2B and is expressed by the conditions applicable in V_{DL} (eq 10) and in V_D (eq 11):[8]

$$(r_p - \ell_{DL}) < r < r_p : \rho = \overline{\rho}_{DL} \quad (10)$$

$$0 < r < (r_p - \ell_{DL}) : \rho = 0 \text{ and } \psi = \psi_D \quad (11)$$

where ρ is the **net** volume charge density in the specified volume domain, and $\bar{\rho}_{DL}$ is the average net volume charge density in the intraparticulate part of the interfacial electric double layer. The characteristic potential distributions invoked in the Poisson-Boltzmann, NICA-Donnan and WHAM models are also illustrated in Fig. 2.

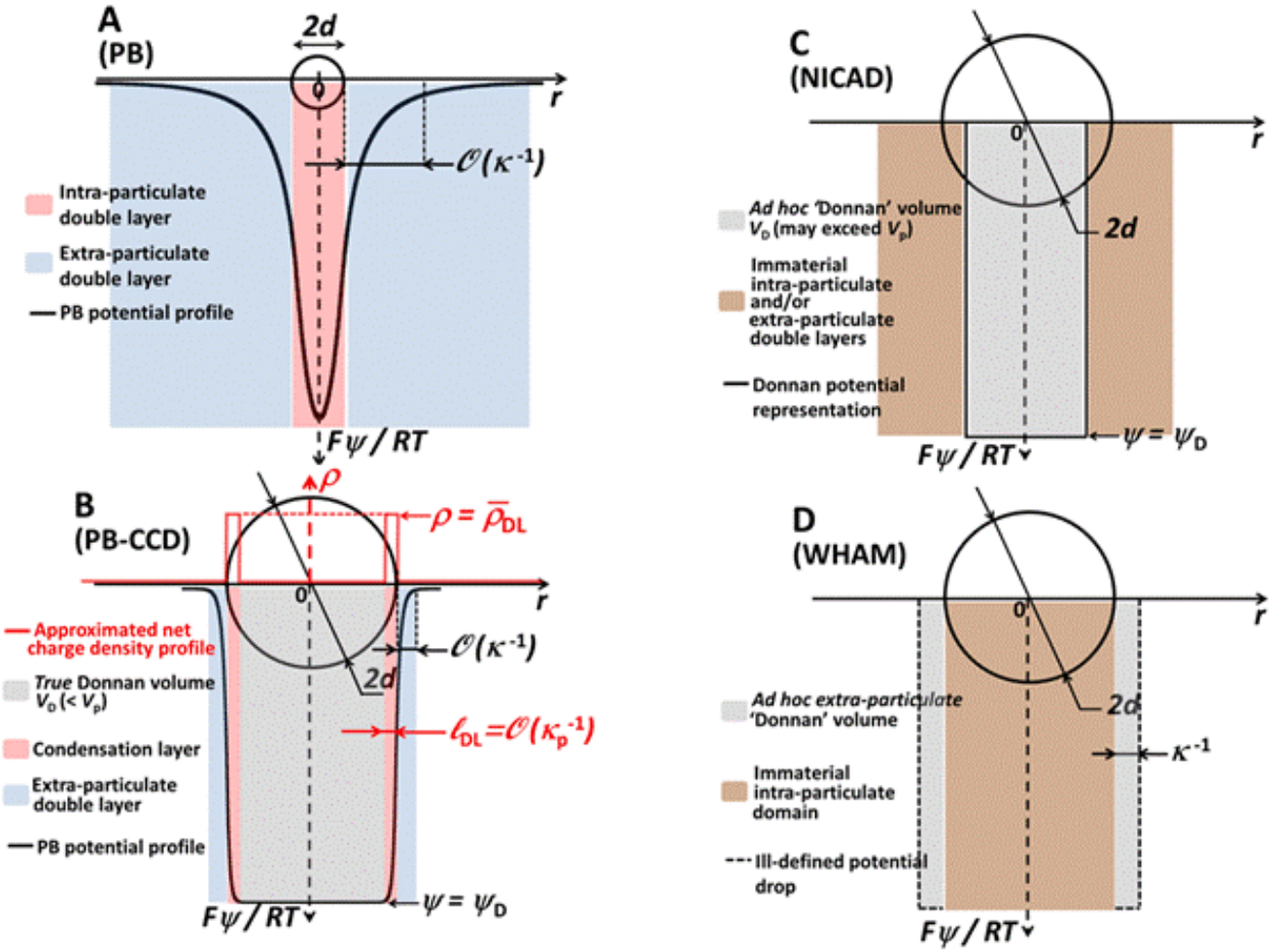

Figure 2. Illustrative potential profiles (in dimensionless form $F\psi / RT$) for highly charged soft nanoparticles computed using various electrostatic models ($d = r_p$; see Fig. 1). (A) Poisson-Boltzmann (PB), as applied to a small NP, $\kappa_p r_p \approx 1$; the extension of the potential profile into the aqueous medium depends on the solution ionic strength. (B) Poisson-Boltzmann – counterion condensation-Donnan (PB-CCD), as applied to a large NP, $\kappa_p r_p >> 1$; the extension of the potential profile into the aqueous medium depends on the solution ionic strength. "$\mathcal{O}$" denotes order of magnitude. (C) NICA-Donnan (NICAD), showing the absence of double layers and the Donnan potential profile, the spatial zone of which is independent of the particle size. (D) WHAM, showing the absence of double layers and the ill-defined extraparticulate Donnan potential profile. See main text for explanation of symbols.

It is pertinent to note that in the CCD approach, for the case $\kappa_p r_p >> 1$ and thus $V_D / V_{DL} >> 1$, the double layer volume can be approximated by using $\ell_{DL} \approx \kappa_p^{-1}$, so that V_{DL} follows as:

$$V_{DL} \approx 4\pi r_p^2 \kappa_p^{-1} \quad (12)$$

and accordingly the Donnan volume can be expressed as:

$$V_D \approx \tfrac{4}{3}\pi r_p^3 - 4\pi r_p^2 \kappa_p^{-1} \quad (13)$$

In the absence of particle swelling/shrinking processes, the ionic strength dependence of V_D is solely contained in κ_p^{-1} via its dependence on κ^{-1} and ψ_D.[55] The ionic strength dependence of ψ_D largely offsets that of κ^{-1}, and thus κ_p^{-1} and the ensuing V_D are practically independent of ionic strength, in line with the starting assumption that $\kappa_p r_p >> 1$.

For the case of humic substances, experimental data obtained by dynamic light scattering (DLS), fluorescence correlation spectroscopy (FCS), and voltammetry show that there is no significant ionic strength- or pH-dependent swelling/contraction of the particles in aqueous dispersions of the order of 100 g m^{-3}. That is, for both HA and FA, of soil and aquatic origins, the average particle size in aqueous dispersion is approximately constant over the pH range 6 to 10 and for ionic strengths up to several 100 mM, indicating no change in the aggregation state within this range.[61,73-75] The finding that diffusion coefficients for HS derived from DLS and FCS measurements are in good agreement with those obtained from electrochemical measurements,[76] demonstrates that these techniques provide a good description of the effective size of HS in aqueous dispersion. Viscosimetric measurements of HS dispersions at concentrations of the order of 2000 g m^{-3} have been interpreted in terms of a solely electrostatics-mediated increase in the hydrated particle size as the ionic strength of the medium decreased.[77] However, use of these results in electrostatic models resulted in poor outcomes.[78] The likely explanation is that the HS size data derived from viscosimetric data[77] are erroneous because the interpretation ignored the potential influence of primary and secondary electroviscous effects. Electroviscous effects are a consequence of electric double layer interactions and interparticulate electrohydrodynamic interactions and can lead to substantial variations in the viscosity of particle dispersions with pH and ionic strength, at *constant* particle size.[79,80] In the CCD approach, the magnitude of ℓ_{DL} is comparable to the thickness of the Manning condensation volume around linear polyionic charges (*ca.* 2 nm),[81] and both f_C and ℓ_{DL} are practically independent of ionic strength,[8,9] in line with Manning's observations for line charges.[65] Consequently, the V_D values employed in the CCD model ($V_D = V_p - V_{DL}$) are also independent of ionic strength. In contrast, the V_D values employed by the NICA-Donnan (eq 6) and WHAM (eq 5) models are inherently ionic strength dependent. A change in V_D amounts to a change in the water content of the particles, and thus a change in the hydrodynamic size. The water content of HA and FA is approximately 80%, regardless of ionic strength.[6,77,82,] The V_D values employed by NICA-Donnan and WHAM, together with the corresponding water contents, are given in Table 2 for a practical range of ionic strengths. The magnitudes of the changes are not supported by experimental observations.[61,73-75] The ionic strength dependencies of V_D assumed by the NICA-Donnan and WHAM models thus lack physicochemical soundness, which seems to be a consequence of the ill-defined nature of the modeling and the associated multi-parametric fitting methodology. The shortcomings of the electrostatic descriptors used in the NICA-Donnan and WHAM models are summarized in Table 3.

Table 2. Donnan volume and percent water content of HA and FA particles as computed by the NICA-Donnan and WHAM models

	I = 100 mM		I = 10 mM		I = 1 mM	
HS sample [a]	V_D dm³/kg	% H_2O	V_D dm³/kg	% H_2O	V_D dm³/kg	% H_2O
NICA-Donnan						
HA, b = 0.49 [b]	0.955	61	2.95	84	9.12	94
HA, b = 0.6 [c]	1.585	72.5	6.31	91	25.1	98
FA, b = 0.57 [b]	1.38	67	5.13	88	19	97
FA, b = 0.35 [d]	0.5	43	1.12	63	2.5	79
WHAM [e]						
HA	2.04	77	8.8	94	59.5	99
FA	5.73	90	65.2	99	1,224	99.95

[a] Computations were performed using an HA density of 1.66 kg dm^{-3} and FA density of 1.5 kg dm^{-3}.[82]

[b] The generic NICA-Donnan b value.[19,83]

[c] The optimised NICA-Donnan b value for Aldrich HA.[84,85]

[d] The optimised NICA-Donnan b value for Laurentian FA.[86]

[e] Computed using the WHAM default particle size for HA (r_p = 1.72 nm) and FA (r_p = 0.8 nm), and κ^{-1} values (eq 2) of 0.9, 2.9, and 9 nm at I = 100, 10, and 1 mM, respectively.

Table 3. Physicochemical shortcomings of the electrostatic descriptors employed in the NICA-Donnan and WHAM models for humic substances

Model	**Inconsistent features of electrostatic descriptors**
NICA-Donnan	• Magnitude of V_D is not constrained by particle size • Extraparticulate Donnan partitioning is allowed, in violation of the Poisson-Boltzmann equation • Ionic strength dependence of V_D is not supported by experimental data • Magnitude of the Donnan potential and Boltzmann partitioning factors is not supported by experimental data • The presence of a highly charged interfacial double-layer is ignored
WHAM VII	• Donnan partitioning is exclusively extraparticulate, in violation of the Poisson-Boltzmann equation • Ionic strength dependence of V_D is not supported by experimental data • Inconsistency between the magnitude of the "Donnan" potential in the extraparticulate zone (with radius κ^{-1}) and the empirical "electrostatic correction factor" (with no defined spatial zone of operation) • The presence of a highly charged interfacial double layer is ignored

3.5. Illustrative example of electrostatic binding: Ca^{2+} association with HA

The physicochemical interactions of Ca^{2+} and Mg^{2+} with negatively charged complexants, such as HS, are dominated by electrostatics,[87,88] yet both NICA-Donnan and WHAM include inner-sphere chemical complexes with finite stability constants, in addition to Donnan partitioning, to describe their binding. For the example case of Ca^{2+} association with Aldrich HA, Table 4 shows the intraparticulate speciation of Ca computed by means of the CCD model and those derived from NICA-Donnan and WHAM.

The physicochemical reasonableness of the V_D values invoked by the speciation models is assessed by computing the intraparticulate aqueous volume of 1 kg of hydrated HA. The reported HA density of 1.66 kg m^{-3} and water content of 80%,[77,82] yields an aqueous volume of 2.5×10^{-3} m^3 kg^{-1}. That is, in a dispersion of 1 kg HA per m^3, there is 2.5 dm^3 of intraparticulate aqueous volume. The physiochemical reasonableness of the V_D values computed by the speciation codes is assessed relative to the magnitude of the intraparticulate aqueous volume. For the case of NICA-Donnan, the dedicated "*b*" value, eq 6, for Aldrich HA is 0.6,[84,85] which corresponds to a V_D of 1.8×10^{-3} m^3 kg^{-1} at an ionic strength of 82 mM. Thus the NICA-Donnan derived V_D is 30% less than that derived from the physicochemical properties of HA. Furthermore, the $\overline{f}_B$ value of 8×10^2 for Ca^{2+} derived from the NICA-Donnan output corresponds to a local charge density of -2,310 mol *e* m^{-3} which is a factor of almost 2 greater than the total value obtained by potentiometric titration.[89] The concentration of inner-sphere Ca complexes predicted by NICA-Donnan corresponds to an intrinsic stability constant of 3.5×10^{-4} m^3 mol^{-1}, which is of comparable magnitude to the stability of an outer-sphere ion pair between 2+ and 1- point charges at the given ionic strength.[90] It thus seems inappropriate to invoke intrinsic chemical binding of Ca^{2+}.[17,19] In the case of WHAM, the intraparticulate aqueous volume of HA is *a priori* zero,[91,92] and it is meaningless to compare the WHAM-derived *extraparticulate* Donnan volume with the physicochemical *intraparticulate* volume. The WHAM-derived $\overline{f}_B$ of 5×10^2 corresponds to the fictive setting of a local charge density of -1,865 mol *e* m^{-3} in the extraparticulate space. Furthermore, the WHAM "electrostatic correction factor", is a factor of *ca*. 20 *lower* than the $\overline{f}_B$ value, underscoring the empirical nature and the disconnect between these two parameters.

The outcome of the NICA-Donnan model is highly dependent on the input parameters. Using parameters that were optimised for Aldrich HA, the model underestimates the experimentally observed degree of association of Ca^{2+}, even though intrinsic chemical binding is invoked, coupled with lower V_D and higher $\overline{f}_B$ values than those expected on the basis of experimental data (Table 4). Use of the generic NICA-Donnan parameters[19,83] yields a better estimate of the concentration of free Ca^{2+} in the bulk medium, but at the cost of the associated V_D and $\overline{f}_B$ being even further from the physicochemically reasonable values (Table 4). Altogether, the outcome points to an inadequate description of the electrostatic contribution to the association of Ca^{2+} with HA by the NICA-Donnan and WHAM models. In contrast, the purely electrostatic CCD model provides a description of the intraparticulate Ca^{2+} speciation that is fairly consistent with the experimental data.

Table 4. Speciation computed in the Ca^{2+}-HA system by CCD, NICA-Donnan, and WHAM models

$c^*_{Ca,t}$ = 0.195 mol m^{-3}, $c^*_{HA,t}$ = 2000 g m^{-3}, pH = 8.2 and I = 82 mol m^{-3} in bulk electrolyte medium.[a]

	CCD[b]	NICA-Donnan		WHAM[e]
		b = 0.49 [c]	b = 0.6 [d]	
$c^*_{Ca,f}$, mol m^{-3}	3.8×10^{-3}	7.07×10^{-3}	3.23×10^{-2}	2.71×10^{-3}
$c_{Ca,t}$, mol m^{-3}	38	89	49.8	43.6
fraction free in V_{DL}	4×10^{-3}	-	-	-
fraction free in V_D	0.03	0.17	0.57	0.03
fraction condensed in V_{DL}	0.97	-	-	-
fraction inner-sphere MS	-	0.83	0.43	0.97
$\overline{f}_B$ in V_D	250	2,196	795	518
aqueous particle volume fraction	5×10^{-3} [f]	2.11×10^{-3} [g]	3.57×10^{-3} [g]	4.41×10^{-3} [g]

[a] Experimental data for Aldrich HA from Hering and Morel.[93]

[b] Computed using the experimentally measured concentration of free Ca^{2+} in the bulk medium,[93] together with a condensation factor, $\overline{f}_C$, of 0.8 in the intraparticulate double layer (DL) with thickness of 2 nm,[8] and a volume charge density of -1,300 mol *e* m^{-3} at pH 8.2.[89] The remaining uncompensated charge in the DL of -260 mol m^{-3} translates to a surface charge density of *ca.* 0.012 C m^{-2} (r_p = 80 nm),[61] corresponding to a potential drop of 34 mV over the distance ℓ_{DL}, which is of the correct order of magnitude,[10] and in line with the difference between the computed Donnan and surface potentials (22 mV, eqs S2 and S3). The intraparticulate DL thickness is similar to the thickness of Manning's counterion condensation volume around linear polyionic charges (*ca.* 2 nm).[81]

[c] Computed using the generic NICA-Donnan parameters for HA[19,83] for the given total concentrations of Ca and HA. The inner-sphere complexes are distributed over the nominal carboxylic (*ca*. 94% of inner-sphere bound) and phenolic groups (*ca.* 6% of inner-sphere bound) at a local pH value of 6.4.

[d] Computed using the NICA-Donnan parameters fitted to Aldrich HA,[84,85] for the given total concentrations of Ca and HA. The inner-sphere complexes are distributed over the nominal carboxylic (*ca*. 70% of inner-sphere bound) and phenolic groups (*ca.* 30% of inner-sphere bound) at a local pH value of 6.6.

[e] Computed using the WHAM VII generic parameters for HA for the given total concentrations of Ca and HA. The inner-sphere complexes are distributed over monodentate (3.5%), bidentate (53.4%), and tridentate (43.1%) species at a local pH of 6.7. The given $\overline{f}_B$ corresponds to the ratio of concentrations of Ca^{2+} in the extraparticulate Donnan layer and in the bulk aqueous media; the "electrostatic correction factor" for these conditions is 25, see text for details.

[f] Computed from the HA density of 1.66 kg dm^{-3} and 80% water content.[77,82]

[g] The aqueous volume fraction of the Donnan phase calculated by the speciation code.

4. INTRINSIC CHEMICAL BINDING AFFINITY

4.1. Intraparticulate metal speciation

The preceding sections highlight the contribution of the particle electric field to the association of counterions with charged NPs such as HS. Depending on the particle size and charge density, the electrostatically associated ions may be present in several different physicochemical forms, *i.e.* free within the extraparticulate double layer, as well as the intraparticulate free, outer-sphere complex, and condensed forms. For metal cations that have an intrinsic chemical affinity for the NP's reactive sites, inner-sphere complex forms will also be present. Proper description of the intrinsic chemical binding parameters for metal complexes with HS *a priori* requires robust accounting for the electrostatic contribution to the extent of metal association. The shortcomings of the WHAM and NICA-Donnan models with regard to description of the particle electrostatic field (detailed in Section 3) inherently mean that the intrinsic chemical affinity parameters are inadequate, as exemplified by Ca^{2+}-HA (Section 3.5).

Once the electrostatic contribution is established, subsequent interpretation of intrinsic metal binding by nanoparticulate complexants such as HS requires proper consideration of the *intraparticulate* conditions within which the metal binding reaction takes place, i.e. the particle electric field and the *local* concentrations of metal ions and reactive sites within the particle body (see Section 2). We have developed well-founded strategies for elucidating the *intraparticulate* metal ion speciation in HS systems, and the intrinsic heterogeneity thereof.[6,94] A characteristic feature of chemically heterogeneous complexants such as HS is that the binding affinity depends on the degree to which the reactive sites are occupied by metal ions, θ_M.[34] We define the true θ_M as the ratio between the *intraparticulate* concentrations of inner-sphere complexes and total reactive sites, *i.e.*:

$$\theta_M = c_{MS} / c_{S,t} \quad (14)$$

The inner-sphere complexes, MS, are constrained to the locations of the reactive sites on the particle surface and/or within the particle body, depending on the type of NP complexant considered (Fig. 1). In contrast, the free metal ion exists both in the bulk aqueous medium and within the electric field of the particle body, and its equilibrium concentration may easily differ by several orders of magnitude between the two domains. The intrinsic stability constant, $\overline{K}_{int}$, represents the inherent chemical affinity between M and a binding site S, *i.e.* not including electrostatic contributions beyond the atom/atom bond distance. The overbar notation signifies that $\overline{K}_{int}$ represents a weighted average of the stabilities of all types of inner-sphere complexes at the given θ_M. In our interpretation framework we define $\overline{K}_{int}$ in terms of the local intraparticulate concentrations of the free metal ion, c_M, inner-sphere complexes, c_{MS}, and reactive sites, c_S, *i.e.*:

$$\overline{K}_{int} = \frac{c_{MS}}{c_M c_S} \quad (15)$$

The electrostatic contributions to the binding can be delineated according to the approaches detailed in the preceding sections, thereby enabling determination of $\overline{K}_{int}$. If details of the particle electric field are not known, then insights can be obtained from experimental measurements in 1-1 and 2-1 electrolytes spanning a range of ionic strengths. At high ionic strength in 2-1 electrolyte (typically 100 mM), present in great excess

over the target divalent metal cation, the electrostatic counterion association is dominated by the divalent cation of the background electrolyte, and the extent of trace metal cation association approaches its intrinsic level.[53] Consistent recovery of the intrinsic binding affinity over a range of 1-1 and 2-1 electrolyte concentrations and θ_M values evidences the robustness of the modelled electrostatic contribution to the binding. This strategy has been used to support the applicability of the Poisson-Boltzmann mean field description of metal ion binding to small soft FA NPs[6] and the CCD description of metal ion binding by large soft HA NPs.[8,9] A description of the involved steps is given in the Supporting Information.

An example of the intraparticulate speciation derived from experimental data for Cd complexes with Aldrich HA using the CCD model is shown in Fig. 3, together with the outcomes derived from the NICA-Donnan and WHAM models. The corresponding figure for the absolute concentration of metal species is given in the Supporting Information, Fig. S1. We note that both speciation codes report the concentrations of all chemical species in the format of smeared-out concentrations, and the only particle-associated metal species are the inner-sphere complexes and the metal ions which are free in V_D. The intraparticulate concentrations in Fig. 3 for NICA-Donnan and WHAM have been derived based on the aqueous volume fraction of the Donnan phase in the dispersion (see section 3.4). Apart from differences in the relative (Fig. 3) and absolute (Fig. S1) concentrations of intraparticulate metal species, the speciation codes differ in their ability to predict the free metal ion concentration in the bulk solution, c^*_{Cd}. The experimentally measured c^*_{Cd} for the conditions shown in Fig. 3 is 3×10^{-4} mM, whilst NICA-Donnan predicts a value of 4.56×10^{-4} mM using the generic parameters and 1.42×10^{-3} mM using the Aldrich optimised parameters, and WHAM predicts a value of 4.74×10^{-4} mM. The NICA-Donnan model together with the generic parameters for HA provides the best estimate of the free metal ion concentration in the bulk medium, yet both the aqueous volume fraction of the HA entities (1.49×10^{-4}) and $\overline{f}_B$ (7,695) are larger than the values derived from experimental data (1.26×10^{-4} and 5,000, respectively). This outcome points to some inadequacies of the NICA-Donnan model in its description of the electrostatic contribution to the association of Cd^{2+} with HA (see also Section 3.5).

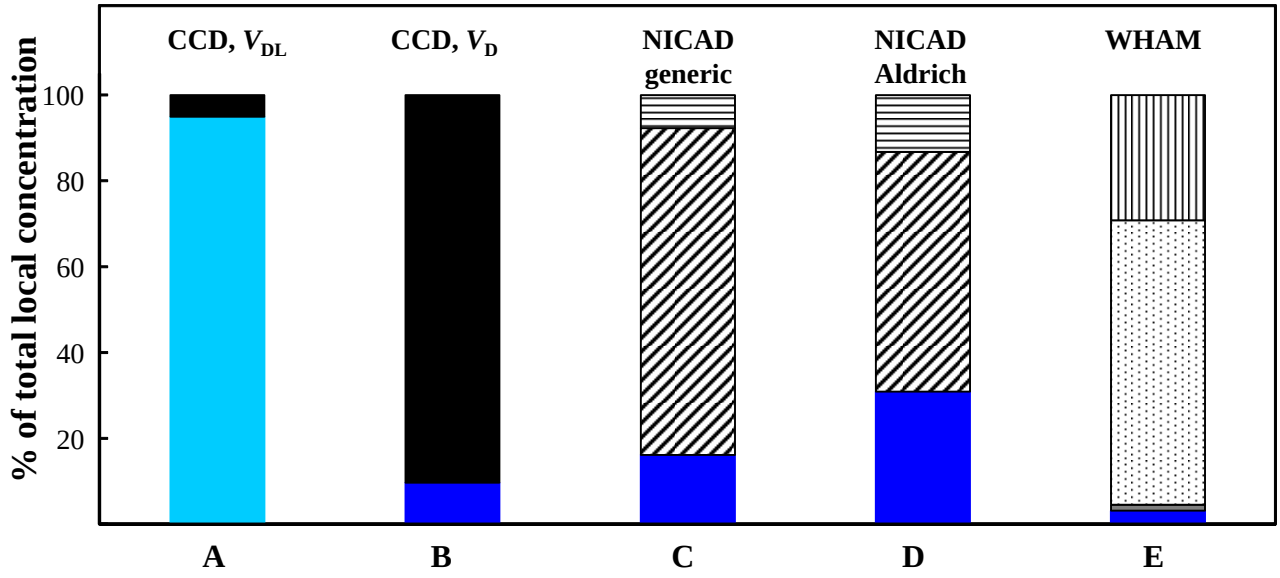

Figure 3. Intraparticulate speciation of Cd(II) associated with Aldrich HA, for a total Cd concentration of 4.6×10^{-3} mM and an HA concentration of 50.5 g m^{-3}, in 10 mM KNO_3 at pH 6. Data correspond to (A) CCD model, intraparticulate part of the interfacial double layer: condensed M (pale blue) and inner-sphere complexes (solid black); (B) CCD model, Donnan volume: free M (dark blue) and inner-sphere complexes (solid black); (C) and (D) NICA-Donnan (NICAD) model using (C) generic[19,83] and (D) Aldrich optimised[84,85] parameters: free M (dark blue) and inner-sphere complexes with nominal carboxylic groups (diagonal stripes) and phenolic groups (horizontal stripes); and (E) WHAM: free M (dark blue) and inner-sphere complexes that are monodentate (solid dark grey), bidentate (black dots), and tridentate (vertical black stripes)

4.2. Chemical heterogeneity of intrinsic metal ion complexation by natural soft HS NPs

Metal ion complexation by humic particles typically features physical and chemical heterogeneities. As discussed above, $\overline{K}_{\mathrm{int}}$ (eq 15) represents the intrinsic binding affinity and θ_{M} (eq 14) denotes the true bound metal-to-binding site ratio. So long as metal ion association with charged NPs does not significantly affect the particle electric field, *i.e.* at sufficiently low θ_{M}, the electrostatic contribution to metal ion binding may be expected to be approximately invariant with θ_{M}. In such case, determination of $\overline{K}_{\mathrm{int}}$ as a function of θ_{M} reveals the inherent heterogeneity in the chemical binding. Specifically, a double logarithmic plot of $\overline{K}_{\mathrm{int}}$ versus θ_{M} for binding of a range of metal ions with fulvic and humic acids yields a straight line with slope equal to $1/\Gamma$, where Γ is the heterogeneity parameter ($0 < \Gamma \leq 1$; $\Gamma = 1$ for the homogeneous case).[6,34,94] It is noteworthy that Γ straightforwardly reflects the metal ion buffer intensity of the system, *i.e.* the change in c_{M}^{*} with change in θ_{M}.[95,96] In the following, we compare the Γ values obtained from double logarithmic $\overline{K}_{\mathrm{int}}$ versus θ_{M} plots derived from our nanoparticle treatment of HS, with independent determinations of Γ by electrochemical measurements, and with the Γ values obtained from the outputs of NICA-Donnan and WHAM.

For comparative purposes herein, the sum of the various inner-sphere complexes computed by the NICA-Donnan and WHAM models was used to compute $\overline{K}_{\mathrm{int}}$ and θ_{M}. The NICA-Donnan and WHAM models incorporate very different ways of accounting for heterogeneity in the chemical binding by humic substances as summarised in Table 1 and references cited therein. Our approach makes no assumptions about the chemical nature of the binding sites, nor the binding stoichiometry; the $\overline{K}_{\mathrm{int}}$, θ_{M} data couples simply follow from eqs 14 and 15 after accounting for the electrostatic contribution to metal ion association (Section 2).

The double logarithmic $\overline{K}_{\mathrm{int}}$ versus θ_{M} plots are shown for HA in Fig. 4 and for FA in Fig. S2. The plots show the $\overline{K}_{\mathrm{int}}$ values derived for HA using the CCD electrostatic model (Fig. 4) and for FA using the mean-field PB approach (Fig. S2), as well as those derived from the output of the NICA-Donnan and WHAM models. It is evident that the various approaches for dealing with the electrostatic contribution to metal ion binding by humic substances eventually yield very different outcomes for the heterogeneity in the chemical binding. The results from the mean-field PB and CCD electrostatic models have been corroborated by independent

551 determination of Γ from the shape of waves constructed from stripping electrochemical measurements over a
552 relevant range of deposition potentials (SSCP).[94,97,98] The shape of an SSCP wave is sensitive to heterogeneity
553 of the metal complex species: the greater the heterogeneity, the more elongated the wave along the potential
554 axis. Figure 4 shows that the Γ values derived from the SSCP waves for CdHA and CuHA are consistent with
555 those obtained from the slope of the log $\overline{K}_{int}$ versus log θ_M plots derived from CCD formalism.[94] The same
556 consistency has been found for FA complexes based on the mean-field PB approach (Fig. S2).[6] In contrast,
557 NICA-Donnan and WHAM modelling lead to heterogeneity parameters, Γ, for both HA (Fig. 4) and FA (Fig.
558 S2) that are not supported by independent experimental electrochemical data,[6,94] and are even impossible in
559 the case of Cd ($\Gamma > 1$). These findings also conflict with the source experimental data used to demonstrate the
560 capabilities of the models, *e.g.* for soil and peat HA at pH 6, a plot of log c_M^* versus log "bound" M has a slope
561 of *ca.* 0.7 for Cd, [17,28] and 0.3 to 0.4 for Cu. [17,84,99]

562 We highlight that the $\overline{K}_{int}$, θ_M data couples, and associated Γ values, arising from our interpretation
563 framework are amenable to incorporation into existing speciation codes. For example, the Visual MINTEQ
564 framework,[100] which currently includes NICA-Donnan parameters, can be adapted to include other modules
565 for handling M-HS interactions, as was envisaged previously for a different type of HS modelling strategy.[101]

566

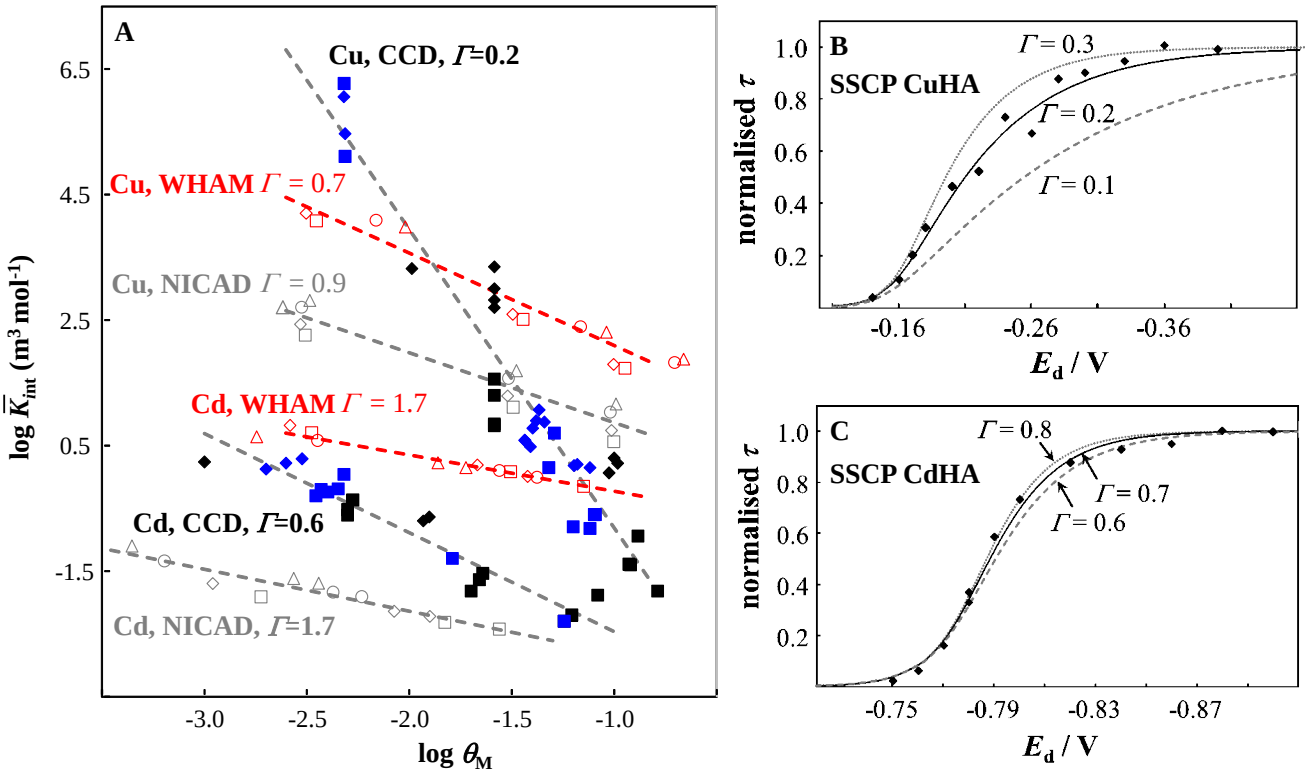

567

568 **Figure 4**. (A) Intrinsic stability constant, log $\overline{K}_{int}$, as function of the degree of inner-sphere complex
569 formation, log θ_M, for Cd(II) and Cu(II) complexes with HA. The CCD-based results were obtained from
570 experimental data for Aldrich HA,[94] obtained in 10 mM KNO_3 (solid black squares), 100 mM KNO_3 (solid
571 black diamonds), 3.33 mM $Ca(NO_3)_2$ (solid blue squares), and 33.33 mM $Ca(NO_3)_2$ (solid blue diamonds).

The NICAD-Donnan computations were done using optimised parameters for Aldrich HA,[84,85] and c_{MS} was taken as the sum of the complexes with the nominal carboxylic and phenolic sites. For WHAM, c_{MS} was taken as the sum of the mono-, bi-, and tri-dentate complexes. The computations with both speciation codes were performed for the background electrolytes 10 mM KNO_3 (NICA-Donnan: open grey squares; WHAM: open red squares), 100 mM KNO_3 (NICA-Donnan: open grey diamonds; WHAM: open red diamonds), 3.33 mM $Ca(NO_3)_2$ (NICA-Donnan: open grey circles; WHAM: open red circles), and 33.33 mM $Ca(NO_3)_2$ (NICA-Donnan: open grey triangles; WHAM: open red triangles). The SSCP waves[94] for (B) CuHA and (C) CdHA correspond to the experimental (solid diamonds) and computed curves for the indicated Γ values (curves) of the normalised reoxidation time, τ, as a function of deposition potential, E_d. The experimental data correspond to $\bar{c}_{M,b} / \bar{c}_{S,t} \approx 0.03$ and were measured in $Ca(NO_3)_2$ electrolyte at pH 6 and ionic strength of 10 mol m^{-3} for CdHA and 100 mol m^{-3} for CuHA.

5. KINETIC FEATURES OF ELECTRIC RELAXATION AND INNER-SPHERE COMPLEXATION; IMPLICATIONS FOR LABILITY AND BIOAVAILABILITY

The previous sections have detailed the electrostatic and intrinsic chemical contributions to the thermodynamic features of metal ion complexes with charged nanoparticulate complexants. In environmental and biological contexts, characterisation of metal-NP complexation needs to go well beyond mere prediction of the free metal ion concentration in the bulk solution: the kinetic features of the metal-NP entities are also fundamentally relevant. Kinetic features of nanoparticulate metal complexes underpin their so-called lability. Lability quantifies the extent to which a metal complex dissociates to release the free metal ion on the timescale of the diffusion of the complex towards an interface that consumes the free metal ion, *e.g.* an analytical sensor or a biointerface.[102] The range of dynamic techniques that are applied to determine metal ion speciation, *e.g.* diffusive gradients in thin film (DGT)[103] and various modes of voltammetry,[104] each operate on a characteristic timescale which is reflected in the range of metal species they are able to determine.[102] Analogously, whilst the bioreactive metal species is often the free metal ion,[105] other metal species may contribute to biouptake if they are able to dissociate on the timescale of the biointerfacial process. Accordingly, the assumption that the equilibrium concentration of the free metal ion is the relevant parameter for predictions of bioavailability is only valid if a number of dynamic criteria are met, *i.e.* mass transfer to the biointerface is not flux-determining, the unsupported diffusion flux of the free metal alone is much larger than the maximum biouptake flux, and there is no bulk depletion.[102,106-112] Indeed, numerous exceptions to equilibrium-based biouptake models have been reported.[113-120] Despite these fundamental issues, there is widespread use of the NICA-Donnan and WHAM speciation codes to compute free metal ion concentrations for use as predictors of bioavailability without verifying compliance with the underlying dynamic criteria.[121-131]

Recent work has elaborated the notion of lability for the case of nanoparticulate complexes and the differences as compared to molecular ones (*e.g.* reaction layer exclusion principles) and the consequences for bioavailability.[33,132,133,] The interpretation is based on an elaboration of the Eigen mechanism, originally derived for describing aqueous metal ion complexation by simple molecular ligands.[134] The approach accounts for the particle electric field, and has been shown to apply to the dissociation/association kinetics of aqueous

609 soft[135] and hard[136] nanoparticulate complexes. For the limiting cases of low and high bulk NP charge densities,
610 expressions are available for the rate constants of the *intraparticulate* outer-sphere and inner-sphere
611 association and dissociation reactions. The chemodynamic framework developed[2,33,38,135] demonstrates that
612 particle shape/size, reactive site density, charge density, and solution ionic strength are key determinants of
613 the dynamic features of the electrostatic and intrinsic chemical binding processes. Notably, the intraparticulate
614 metal speciation underpins the kinetic features, *e.g*. intraparticulate free metal ions may be released from the
615 particle on a timescale different from those that are inner-sphere bound, *e.g.* as a result of a limited dissociation
616 rate. NP reactivity theory enables identification of the various limiting cases in the rate of the intraparticulate
617 complex formation/dissociation processes.[137] The overall reaction rate is determined by the relative timescales
618 of the involved electric and chemical relaxation processes.[33]

619 In terms of electric relaxation for the highly charged complexing nanoparticle with an intraparticulate Donnan
620 volume ($\kappa_p r_p >> 1$) in an aqueous medium with a background electrolyte at a concentration much higher than
621 that of the target reactant metal ion, the complete electric equilibration of the ionic partitioning over the
622 medium and nanoparticle phases generally is of a differentiated nature. In early stages of the relaxation in a
623 sufficiently diluted dispersion of NPs (no significant depletion of metal from the medium), all types of ions
624 contribute in accordance with their concentrations and mobilities: for a negatively charged NP the positive
625 counterions diffuse from the medium towards the NP, whereas the coions diffuse in the opposite direction.
626 Upon approach of the electric equilibrium state, differences between various types of counterions give rise to
627 slower exchange processes, *e.g.* the replacement of bound 1+ ions by the more attractive 2+ ions. Something
628 similar occurs in electrochemical processes with electroactive reactants in an excess background electrolytic
629 medium.[138] For spherical NPs, relaxation time constants for partitioning of counterionic species are typically
630 on the order of r_p^2 / D_{ion}, where D_{ion} is the ion diffusion coefficient. For aqueous cations with D_{ion} on the
631 order of 10^{-9} m^2 s^{-1} and NPs with radii of 10 nm this comes to the order of 10^{-7} s. In sorting out the establishment
632 of full equilibration, such relaxation times are to be set against other typical times such as those for inner-
633 sphere complex formation.[33] Equilibrium speciation codes generally do not verify the correctness of assuming
634 full equilibrium. For more details, the reader is referred to ref. 139.

635 The previous sections have highlighted the shortcomings of the NICA-Donnan and WHAM speciation codes
636 in regard to predicting equilibrium metal speciation in the presence of humic substances. Whilst in some cases
637 the predicted free metal ion concentration in the bulk solution was in reasonable agreement with experimental
638 data, some of the associated fitting parameters did not possess physicochemically reasonable magnitudes and
639 thus the derived intraparticulate metal speciation is likely to be erroneous. Furthermore, in the case of field
640 studies on freshwaters, the free metal ion concentrations predicted by both NICA-Donnan and WHAM are
641 reported to be in poor agreement with data from *in situ* measurements, especially at low free metal ion
642 concentrations and for metal ions that associate strongly with HS, e.g. Cu^{2+}.[140-143] This outcome reflects the
643 empirical nature of the model parameters and their inability to account for heterogeneity in the complexation
644 over a suitably wide range. It follows that attempts to correlate metal speciation computed by these codes to

dynamic features such as lability,[144-153] bioavailability and/or toxicity[121-131] are bound to suffer from physicochemically poor outcomes.

6. CONCLUSIONS AND OUTLOOK

Our analysis of metal ion binding to nanoparticulate humic substances as predicted by the NICA-Donnan and WHAM speciation models shows that the physicochemical meaning of the outcome is questionable due to the empirical nature of various key parameters used in these models and the ambiguous nature of the fitting process. For example, if NICA-Donnan is allowed to optimize the fit to experimental data by varying its constituent parameters, the model can provide a good description of the free metal ion concentration in the presence of HA over a wide range of conditions.[17,18] However, the physicochemical meaning of the resulting parameters is not transparent because the fitting process concomitantly optimizes the interrelated sub-models for intrinsic chemical and electrostatic binding components.[19] Indeed, a recent review of the NICA-Donnan approach stated ''The fact that a set of parameter values can be non-unique is first of all due to the large number of parameters in the model. A different way of fitting of the parameters to the data may lead to an equally good description of the data, but different parameter values.''[58] This situation is particularly problematic for cases in which more than the mere free M in the bulk solution is of interest. For example, prediction of the potential bioavailability of metal species inherently involves consideration of their kinetic features. The fundamental starting point for such an approach is knowledge of the nature, concentration, stability, and heterogeneity of the various particle associated forms, and the dynamic nature of competition between the various intraparticulate physicochemical forms of M. It is clear that efforts to model metal ion association with charged nanoparticulate complexants require proper formulation of the particle electric field distribution for the given particle size and charge density characteristics. In the absence of this foundation, any descriptors of the intrinsic chemical affinity are bound to be inadequate. In particular, proper description of the electric field in the extraparticulate and intraparticulate parts of the interfacial double layers of charged NPs has been largely overlooked in the context of environmental nanoparticulate complexants. In this context we are developing more rigorous theory to define the intraparticulate double layer thickness in soft charged NPs and the 3D electrostatic counterion condensation phenomena therein. Future work will need to focus on application of the current knowledge on the reactivity of nanoparticulate HS complexants to removal of physicochemical shortcomings from existing equilibrium speciation codes. The parameters we derive herein, i.e. electrostatic descriptors and $\overline{K}_{\mathrm{int}}$, θ_{M} couples, are amenable to incorporation into such codes, following previously envisaged strategies,[101] and we are pursuing such developments. It follows that empirical correlations between equilibrium chemical speciation and bioavailability and/or toxicity will need to be revisited in light of the new knowledge, and properly upgraded to include the dynamics of redistribution of intraparticulate (bio)reactive metal species. Work is underway to extend the interpretation framework to account for *e.g.* the effects of:

- particle shape,
- intraparticulate physical and chemical heterogeneities,
- intraparticulate competition between condensed and free forms of different types of metal ions, and
- random versus allocated charge distributions

on the stability and reactivity of inner-sphere nanoparticulate metal complexes.

ASSOCIATED CONTENT

Supporting Information

The Supporting Information is available free of charge on the ACS Publications website at DOI: xxx

The Supporting Information includes an outline of the Ohshima formalism for the electrophoretic mobility of soft charged particles, description of the procedures used to obtain the intrinsic stability constants for metal ion binding by nanoparticulate complexants, Table S1 with definitions of the parameters used in the CCD-based model, Figure S1 showing the intraparticulate speciation of Cd species associated with Aldrich HA, Figure S2 showing the double logarithmic plot of $\overline{K}_{\mathrm{int}}$ *vs.* θ_{M} and SSCP waves for Cd(II) and Cu(II) complexes with FA, and a list of the references cited in the SI.

ACKNOWLEDGEMENTS

RMT conducted this work within the framework of the EnviroStress Centre of Excellence at the University of Antwerp.

The authors declare no competing financial interest.

REFERENCES

(1) Pinheiro, J. P.; Minor, M.; van Leeuwen, H. P. Metal speciation dynamics in colloidal ligand dispersions. *Langmuir* **2005**, *21*, 8635-8642.

(2) van Leeuwen, H. P.; Buffle, J. Chemodynamics of aquatic metal complexes: from small ligands to colloids. *Environ. Sci. Technol*. **2009**, *43*, 7175-7183.

(3) van Leeuwen, H. P.; Buffle, J.; Duval, J. F. L; Town, R. M. Understanding the extraordinary ionic reactivity of aqueous nanoparticles. *Langmuir* **2013**, *29*, 10297-10302.

(4) Wonders, J. H. A. M.; van Leeuwen, H. P. Voltammetric metal titration of particle dispersions. *J. Electroanal. Chem.* **1996**, *401*, 103-112.

(5) Duval, J. F. L.; Farinha, J. P. S.; Pinheiro, J. P. Impact of electrostatics on the chemodynamics of highly charged metal-polymer nanoparticle complexes. *Langmuir* **2013**, *29*, 13821-13835.

(6) Town, R. M.; Duval, J. F. L.; van Leeuwen, H. P. The intrinsic stability of metal ion complexes with nanoparticulate fulvic acids. *Environ. Sci. Technol.* **2018**, *52*, 11682-11690.

(7) van Leeuwen, H. P.; Town, R. M. Electric condensation of divalent counterions by humic acid nanoparticles. *Environ. Chem.* **2016**, *13*, 76-83.

(8) Town, R. M.; van Leeuwen, H. P. Intraparticulate speciation analysis of soft nanoparticulate metal complexes. The impact of electric condensation on the binding of Cd^{2+}/Pb^{2+}/Cu^{2+} by humic acids. *Phys. Chem. Chem. Phys.* **2016**, *18*, 10049-10058.

(9) Town, R. M.; van Leeuwen, H. P. Metal ion – humic acid nanoparticle interactions: role of both complexation and condensation mechanisms. *Phys. Chem. Chem. Phys.* **2016**, *18*, 18024-18032.

(10) Duval, J. F. L.; Wilkinson, K. J.; van Leeuwen, H. P.; Buffle, J. Humic substances are soft and permeable: evidence from their electrophoretic mobilities. *Environ. Sci. Technol.* **2005**, *39*, 6435-6445.

(11) Sutton, R.; Sposito, G. Molecular structure in soil humic substances: the new view. *Environ. Sci. Technol.* **2005**, *39*, 9009-9015.

(12) Klučáková, M.; Věžníková, K. Micro-organization of humic acids in aqueous solutions. *J. Molec. Sci.* **2017**, *1144*, 33-40.

(13) Wells, M. J. M.; Stretz, H. A. Supramolecular architectures of natural organic matter. *Sci. Total Environ.* **2019**, *671*, 1125-1133.

(14) Herzsprung, P.; Hertkorn, N.; von Tümpling, W.; Harir, M.; Friese, K.; Schmitt-Kopplin, P. 2014. Understanding molecular formula assignment of Fourier transform ion cyclotron resonance mass spectrometry data of natural organic matter from a chemical point of view. *Anal. Bioanal. Chem.* **2014**, *406*, 7977-7987.

(15) Kunenkov, E. V.; Kononikhin, A. S.; Perminova, I. V.; Hertkorn, N.; Gaspar, A.; Schmitt-Kopplin, P.; Popov, I. A.; Garmash, A. V.; Nikolaev, E. N. Total mass difference statistics algorithm: a new approach to identification of high-mass building blocks in electrospray ionization Fourier transform ion cyclotron mass spectrometry data of natural organic matter. *Anal. Chem.* **2009**, *81*, 10106-10115.

(16) Petrov, D.; Tunega, D.; Gerzabek, M. H.; Oostenbrink, C. Molecular dynamics simulations of the standard Leonardite humic acid: microscopic analysis of the structure and dynamics. *Environ. Sci. Technol.* **2017**, *51*, 5414-5424.

(17) Benedetti, M. F.; Milne, C. J.; Kinniburgh, D. G.; van Riemsdijk, W. H.; Koopal, L. K. Metal ion binding to humic substances: application of the non-ideal competitive adsorption model. *Environ. Sci. Technol.* **1995**, *29*, 446-457.

(18) Christl, I.; Milne, C. J.; Kinniburgh, D. G.; Kretzschmar, R. Relating ion binding by fulvic and humic acids to chemical composition and molecular size. 2. Metal binding. *Environ. Sci. Technol.* **2001**, *35*, 2512-2517.

(19) Milne, C. J.; Kinniburgh, D. G.; van Riemsdijk, W. H.; Tipping, E. Generic NICA-Donnan model parameters for metal-ion binding by humic substances. *Environ. Sci. Technol.* **2003**, *37*, 958-971.

(20) Tipping, E. Humic-ion binding model VI: an improved description of the interaction of protons and metal ions with humic substances. *Aquat. Geochem.* **1998**, *4*, 3-48.

(21) Tipping, E.; Lofts, S.; Sonke, J. E. Humic ion-binding model VII: a revised parameterisation of cation-binding by humic substances. *Environ. Chem.* **2011**, *8*, 225-235.

(22) Tipping, E.; Backes, C. A.; Hurley, M. A. The complexation of protons, aluminium and calcium by aquatic humic substances: a model incorporating binding-site heterogeneity and macroionic effects. *Water Res.* **1988**, *22*, 597-611.

(23) De Wit, J. C. M.; van Riemsdijk, W. H.; Nederlof, M. M.; Kinniburgh, D. G.; Koopal, L. K. Analysis of ion binding on humic substances and the determination of intrinsic affinity distributions. *Anal. Chim. Acta* **1990**, *232*, 189-207.

(24) Nederlof, M. M.; van Riemsdijk, W. H.; Koopal, L. K. Comparison of semianalytical methods to analyze complexation with heterogeneous ligands. *Environ. Sci. Technol.* **1992**, *26*, 763-771.

(25) De Wit, J. C. M.; Nederlof, M. M.; van Riemsdijk, W. H.; Koopal, L. K. Determination of hydrogen ion and metal ion affinity distributions for humic substances. *Water Air Soil Poll.* **1991**, *57-58*, 339-349.

(26) Weng, L.; Temminghoff, E. J. M.; Lofts, S.; Tipping, E.; van Riemsdijk, W. H. Complexation with dissolved organic matter and solubility control of heavy metals in a sandy soil. *Environ. Sci. Technol.* **2002**, *36*, 4804-4810.

(27) Ahmed, I. A. M.; Hamilton-Taylor, J.; Lofts, S.; Meeussen, J. C. L.; Lin, C.; Zhang, H.; Davison, W. Testing copper-speciation predictions in freshwaters over a wide range of metal-organic matter ratios. *Environ. Sci. Technol.* **2013**, *47*, 1487-1495.

(28) Kinniburgh, D. G.; van Riemsdijk, W. H.; Koopal, L. K.; Borkovec, M.; Benedetti, M. F.; Avena, M. J. Ion binding to natural organic matter: competition, heterogeneity, stoichiometry and thermodynamic consistency. *Colloids Surf. A* **1999**, *151*, 147-166.

(29) Puy, J.; Huidobro, C.; David, C.; Rey-Castro, C.; Salvador, J.; Companys, E.; Garcés, J. L.; Galceran, J.; Cecília, J.; Mas, F. Conditional affinity spectra underlying the NICA isotherm. *Colloids Surf. A: Physicochem. Eng. Aspects* **2009**, *347*, 156-166.

(30) van Riemsdijk, W. H.; Koopal, L. K.; Kinniburgh, D. G.; Benedetti, M. F.; Weng, L. Modeling the interactions between humics, ions, and mineral surfaces. *Environ. Sci. Technol.* **2006**, *40*, 7473-7480.

(31) Carbonaro, R. F.; Di Toro, D. M. Linear free energy relationships for metal-ligand complexation: monodentate binding to negatively-charged oxygen donor atoms. *Geochim. Cosmochim. Acta* **2007**, *71*, 3958-3968.

(32) Carbonaro R. F.; Atalay, Y. B.; Di Toro, D. M. Linear free energy relationships for metal-ligand complexation: bidendate binding to negatively-charged oxygen donor atoms. *Geochim. Cosmochim. Acta* **2011**, *75*, 2499-2511.

(33) van Leeuwen, H. P.; Duval, J. F. L.; Pinheiro, J. P.; Blust, R.; Town, R. M. Chemodynamics and bioavailability of metal ion complexes with nanoparticles in aqueous media. *Environ. Sci.: Nano* **2017**, *4*, 2108-2133.

(34) Buffle, J. *Complexation Reactions in Aquatic Systems. An Analytical Approach.* Ellis Horwood: Chichester, 1988.

(35) Buffle, J.; Zhang, Z.; Startchev, K. Metal flux and dynamic speciation at (bio)interfaces. Part I: Critical evaluation and compilation of physiochemical parameters for complexes with simple ligands and fulvic/humic substances. *Environ. Sci. Technol.* **2007**, *41*, 7609-7620.

(36) Marshall, S. J.; Young, S. D.; Gregson, K. Humic acid-proton equilibria: a comparison of two models and assessment of titration error. *Eur. J. Soil. Sci.* **1995**, *46*, 471-480.

(37) Town, R. M.; Buffle, J.; Duval, J. F. L.; van Leeuwen, H. P. Chemodynamics of soft charged nanoparticles in aquatic media: fundamental concepts. *J. Phys. Chem. A* **2013**, *117*, 7643-7654.

(38) Duval, J. F. L. Chemodynamics of metal ion complexation by charged nanoparticles: a dimensionless rationale for soft, core-shell and hard particle types. *Phys. Chem. Chem. Phys.* **2017**, *19*, 11802-11815.

(39) Ohshima, H. Electrophoresis of soft particles. *Adv. Colloid Interf. Sci.* **1995**, *62*, 189-235.

(40) Delgado, A. V.; González-Caballero, F.; Hunter, R. J.; Koopal, L. K.; Lyklema, J. Measurement and interpretation of electrokinetic phenomena. *J. Colloid Interf. Sci.* **2007**, *309*, 194-224.

(41) O'Brien, R. W.; White, L. R. Electrophoretic mobility of a spherical colloidal particle. *J. Chem. Soc. Faraday Trans. II.* **1978**, *74*, 1607-1626.

(42) Duval, J. F. L.; Gaboriaud, F. Progress in electrohydrodynamics of soft microbial particle interphases. *Curr. Opinion Coll. Interf. Sci.* **2010**, *15*, 184-195.

(43) Duval, J. F. L. Electrophoresis of soft colloids: basic principles and applications. In: *Environmental Colloids and Particles: Behaviour, Separation and Characterisation*. Wilkinson, K. J. and Lead, J. R. (Vol. Eds), IUPAC Series on Analytical and Physical Chemistry of Environmental Systems, Vol. 10, Buffle, J. and van Leeuwen, H. P. (Series Eds), John Wiley & Sons Ltd: Chichester, 2007, pp. 315-344.

(44) Hill, R. J.; Saville, D. A.; Russel, W. B. Electrophoresis of spherical polymer-coated particles. *J. Coll. Interf. Sci.* **2003**, *258*, 56-74.

(45) Duval, J. F. L.; Ohshima, H. Electrophoresis of diffuse soft particles. *Langmuir* **2006**, *22*, 3533-3546.

(46) Martin, J. R. S.; Bihannic, I.; Santos, C.; Farinha, J. P. S.; Demé, B.; Leermakers, F. A. M.; Pinheiro, J. P.; Rotureau, E.; Duval, J. F. L. Structure of multiresponsive brush-decorated nanoparticles: a combined electrokinetic, DLS, and SANS study. *Langmuir* **2015**, *31*, 4779-4790.

(47) Ai, Y.; Qian, S. Direct numerical simulation of electrokinetic translocation of a cylindrical particle through a nanopore using a Poisson-Boltzmann approach. *Electrophoresis* **2011**, *32*, 996-1005.

(48) Ohshima, H. A simple algorithm for the calculation of an approximate electrophoretic mobility of a spherical colloidal particle based on the modified Poisson-Boltzmann equation. *Coll. Polym. Sci.* **2017**, *295*, 543-548.

(49) Duval, J. F. L.; van Leeuwen, H. P. Rates of ionic reactions with charged nanoparticles in aqueous media. *J. Phys. Chem. A* **2012**, *116*, 6443-6451.

(50) Deserno, M.; Holm, C.; May, S. Comparison of Poisson-Boltzmann theory and computer simulations. *Macromolecules* **2000**, *33*, 199-206.

(51) Ben-Yaakov, D.; Andelman, D.; Harries, D.; Podgornik, R. Beyond standard Poisson-Boltzmann theory: ion-specific interactions in aqueous solutions. *J. Phys.: Condens. Matter* **2009**, *21*: 424106.

(52) Moussa, M.; Caillet, C.; Town, R. M.; Duval, J. F. L. Remarkable electrokinetic features of charge-stratified soft nanoparticles: mobility reversal in monovalent aqueous electrolyte. *Langmuir* **2015**, *31*, 5656-5666.

(53) Duval, J. F. L.; Town, R. M.; van Leeuwen, H. P. Poisson-Boltzmann electrostatics and ionic partition equilibration of charged nanoparticles in aqueous media. *J. Phys. Chem. C* **2018**, *122*, 17328-17337.

(54) Duval, J. F. L.; van Leeuwen, H. P. Electrokinetics of diffuse soft interfaces. I. Limit of low Donnan potentials. *Langmuir* **2004**, *20*, 10324-10336.

(55) Duval, J. F. L. Electrokinetics of diffuse soft interfaces. II. Analysis based on the nonlinear Poisson-Boltzmann equation. *Langmuir* **2005**, *21*, 3247-3258.

(56) Ohshima, H.; Kondo, T. Relationship among the surface potential, Donnan potential and charge density of ion-penetrable membranes. *Biophys. Chem.* **1990**, *38*, 117-122.

(57) Yezek, L. P.; van Leeuwen, H. P. Donnan effects in the steady-state diffusion of metal ions through charged thin films. *Langmuir* **2005**, *21*, 10342-10347.

(58) Koopal, L. K.; Saito, T.; Pinheiro, J. P.; van Riemsdijk, W. H. Ion binding to natural organic matter: general considerations and the NICA-Donnan model. *Colloids and Surfaces A* **2005**, *265*, 40-54.

(59) Companys, E.; Garcés, J. L.; Salvador, J.; Galceran, J.; Puy, J.; Mas, F. Electrostatic and specific binding to macromolecular ligands. A general analytical expression for the Donnan volume. *Coll. Surf. A* **2007**, *306*, 2-13.

(60) Benedetti, M. F.; van Riemsdijk, W; H.; Koopal, L. K. Humic substances considered as a heterogeneous Donnan gel phase. *Environ. Sci. Technol.* **1996**, *30*, 1805-1813.

(61) Tan, W. F.; Koopal, L. K.; Norde, W. Interaction between humic acid and lysozyme, studied by dynamic light scattering and isothermal titration calorimetry. *Environ. Sci. Technol.* **2009**, *43*, 591-596.

(62) Pinheiro, J. P.; Mota, A. M.; d'Oliveira, J. M. R.; Martinho, J. M. G. Dynamic properties of humic matter by dynamic light scattering and voltammetry. *Anal. Chim. Acta* **1996**, *329*, 15-24.

(63) Hosse, M.; Wilkinson, K. J. Determination of electrophoretic mobilities and hydrodynamic radii of three humic substances as a function of pH and ionic strength. *Environ. Sci. Technol.* **2001**, *35*, 4301-4306.

(64) Lenoir, T.; Matynia, A.; Manceau, A. Convergence-optimized procedure for applying the NICA-Donnan model to potentiometric titrations of humic substances. *Environ. Sci. Technol.* **2010**, *44*, 6221-6227.

(65) Manning, G. S. Counterion binding in polyelectrolyte theory. *Acc. Chem. Res.* **1979**, *12*, 443-449.

(66) Manning, G. S. Limiting laws and counterion condensation in polyelectrolyte solutions. I. Colligative properties. *J. Chem. Phys.* **1969**, *51*, 924-933.

(67) Garcia-Fernandez, E.; Paulo, P. M. R.; Costa, S. M. B. Evaluation of electrostatic binding of PAMAM dendrimers and charged phthalocyanines by fluorescence correlation spectroscopy. *Phys. Chem. Chem. Phys.* **2015**, *17*, 4319-4327.

(68) Majtyka, M.; Kłos, J. Monte Carlo simulation of a charged dendrimer with explicit counterions and salt ions. *Phys. Chem. Chem. Phys.* **2007**, *9*, 2284-2292.

(69) Huang, Q. R.; Dubin, P. L.; Moorefield, C. N.; Newkome, G. R. Counterion binding on charged spheres: effect of pH and ionic strength on the mobility of carboxyl-terminated dendrimers. *J Phys. Chem. B* **2000**, *104*, 898-904.

(70) Li, Z.; van Dyk, A. K.; Fitzwater, S. J.; Fichthorn, K. A.; Milner, S. T. Atomistic molecular dynamics simulations of charged latex particle surfaces in aqueous solution. *Langmuir* **2016**, *32*, 428-441.

(71) Manning, G. S. The molecular theory of polyelectrolyte solutions with applications to the electrostatic properties of polynucleotides. *Q. Rev. Biophys.* **1978**, *11*, 179-246.

(72) van Leeuwen, H. P.; Cleven, R. F. M. J.; Valenta, P. Conductometric analysis of polyelectrolytes in solution. *Pure Appl. Chem.* **1991**, *63*, 1251-1268.

(73) Pinheiro, J. P.; Mota, A. M.; d'Oliveira, J. M. R.; Martinho, J. M. G. Dynamic properties of humic matter by dynamic light scattering and voltammetry. *Anal. Chim. Acta* **1996**, *329*, 15-24.

(74) Lead, J. R.; Wilkinson, K. J.; Starchev, K.; Canonica, S.; Buffle, J. Determination of diffusion coefficients of humic substances by fluorescence correlation spectroscopy: role of solution conditions. *Environ. Sci. Technol.* **2000**, *34*, 1365-1369.

(75) Hosse, M.; Wilkinson, K. J. Determination of electrophoretic mobilities and hydrodynamic radii of three humic substances as a function of pH and ionic strength. *Environ. Sci. Technol.* **2001**, *35*, 4301-4306.

(76) Pinheiro, J. P.; Domingos, R.; Lopez, R.; Brayner, R.; Fiévet, F.; Wilkinson, K. Determination of diffusion coefficients of nanoparticles and humic substances using scanning stripping chronopotentioemetry (SSCP). *Coll. Surf. A: Physicochem. Eng. Aspects* **2007**, *295*, 200-208.

(77) Avena, M. J.; Vermeer, A. W. P.; Koopal, L. K. Volume and structure of humic acids studied by viscometry pH and electrolyte concentration effects. *Coll. Surf. A: Physicochem. Eng. Apects* **1999**, *151*, 213-224.

(78) Saito, T.; Nagasaki, S.; Tanaka, S.; Koopal, L. K. Electrostatic interaction models for ion binding to humic substances. *Coll. Surf. A: Physicochem. Eng. Aspects* **2005**, *265*, 104-113.

(79) Zurita, L.; Carrique, F.; Delgado, A. V. The primary electroviscous effect in silica suspensions. Ionic strength and pH effects. *Coll. Surf. A: Physicochem. Eng. Aspects* **1994**, *92*, 23-28.

(80) Chan, F. S.; Blachford, J.; Goring, D. A. I. The secondary electroviscous effect in a charged spherical colloid. *J. Coll. Interf. Sci.* **1966**, *22*, 378-385.

(81) Manning, G. S. Limiting laws and counterion condensation in polyelectrolyte solutions. IV. The approach to the limit and the extraordinary stability of the charge fraction. *Biophys. Chem.* **1977**, *7*, 95-102.

(82) Dinar, E.; Mentel, T. F.; Rudich, Y. The density of humic acids and humic like substances (HULIS) from fresh and aged wood burning and pollution aerosol particles. *Atmos. Chem. Phys.* **2006**, *6*, 5213-5224.

(83) Milne, C. J.; Kinniburgh, D. G.; Tipping, E. Generic NICA-Donnan model parameters for proton binding by humic substances. *Environ. Sci. Technol.* **2001**, *35*, 2049-2059.

(84) Tan, W.; Xiong, J.; Li, Y.; Wang, M.; Weng, L.; Koopal, L. K. Proton binding to soil humic and fulvic acids: experiments and NICA-Donnan modelling. *Coll. Surf. A: Physiochem. Eng. Aspects* **2013**, *436*, 1152-1158.

(85) Xu, J.. Tan, W.; Xiong, J.; Wang, M.; Fang, L.; Koopal, L. K. Copper binding to soil fulvic and humic acids: NICA-Donnan modeling and conditional affinity spectra. *J. Coll. Interf. Sci.* **2016**, *473*, 141-151.

(86) Janot, N.; Pinheiro, J. P.; Botero, W. G.; Meeussen, J. C. L.; Groenenberg, J. E. PEST-ORCHESTRA, a tool for optimising advanced ion-binding model parameters: derivation of NICA-Donnan model parameters for humic substances reactivity. *Environ. Chem.* **2017**, *14*, 31-38.

(87) Krishnan, K.; Plane, R. A. Raman spectra of ethylenediaminetetraacetic acid and its metal complexes. *J. Am. Chem. Soc.* **1968**, *90*, 3195-3200.

(88) Clapp, L. A.; Siddons, C. J. Whitehead, J. R.; van Derveer, D. G.; Rogers, R. D.; Griffin, S. T.; Jones, S. B.; Hancock, R. D. Factors controlling metal-ion selectivity in the binding sites of calcium-binding proteins. The metal-binding properties of amide donors. A crystallographic and thermodynamic study. *Inorg. Chem.* **2005**, *44*, 8495-8502.

(89) Tan, W. -F.; Norde, W.; Koopal, L. K. Humic substance charge determination by titration with a flexible cationic polyelectrolyte. *Geochim. Cosmochim. Acta* **2011**, *75*, 5749-5761.

(90) Fuoss, R. M. Ionic association. III. The equilibrium between ion pairs and free ions. *J. Am. Chem. Soc.* **1958**, *80*, 5059-5061.

(91) Tipping, E.; Backes, C. A.; Hurley, M. A. The complexation of protons, aluminium and calcium by aquatic humic substances: a model incorporating binding-site heterogeneity and macroionic effects. *Wat. Res.* **1988**, *22*, 597-611.

(92) Tipping, E.; Reddy, M. M.; Hurley, M. A. Modeling electrostatic and heterogeneity effects on proton dissociation from humic substances. *Environ. Sci. Technol.* **1990**, *24*, 1700-1705.

(93) Hering, J. G.; Morel, F. M. M. Humic acid complexation of calcium and copper. *Environ. Sci. Technol.* **1988**, *22*, 1234-1237.

(94) Town, R. M.; van Leeuwen, H. P. Intraparticulate metal speciation analysis of soft complexing nanoparticles. The intrinsic chemical heterogeneity of metal-humic acid complexes. *J. Phys. Chem. A* **2016**, *120*, 8637-8644.

(95) Buffle, J.; Altmann, R. S.; Filella, M. Effect of physico-chemical heterogeneity of natural complexants. Part II. Buffering action and role of their background sites. *Anal. Chim. Acta* **1990**, *232*, 225-237.

(96) Buffle, J.; Altmann, R. S.; Filella, M.; Tessier, A. Complexation by natural heterogeneous compounds: site occupation distribution functions, a normalized description of metal complexation. *Geochim. Cosmochim. Acta* **1990**, *54*, 1535-1553.

(97) Town, R. M.; van Leeuwen, H. P. Dynamic speciation analysis of heterogeneous metal complexes with natural ligands by SSCP (stripping chronopotentiometry at scanned deposition potential). *Aust. J. Chem.* **2004**, *57*, 983-992.

(98) van Leeuwen, H. P.; Town, R. M. Electrochemical metal speciation analysis of chemically heterogeneous samples: the outstanding features of stripping chronopotentiometry at scanned deposition potential. *Environ. Sci. Technol.* **2003**, *37*, 3945-3952.

(99) Vidali, R.; Remoundaki, E.; Tsezos, M. An experimental and modelling study of Cu^{2+} binding on humic acids at various solution conditions. Application of the NICA-Donnan model. *Water Air Soil Pollut.* **2011**, *218*, 487-497.

(100) Gustafsson, J. P. Visual MINTEQ. Open access software available at https://vminteq.lwr.kth.se/

(101) Huber, C.; Filella, M.; Town, R. M. Computer modelling of trace metal ion speciation: practical implementation of a linear continuous function for complexation by natural organic matter. *Comp. Geosci.* **2002**, *28*, 587-596.

(102) van Leeuwen, H. P.; Town, R. M.; Buffle, J.; Cleven, R. F. M. J.; Davison, W.; Puy, J.; van Riemsdijk, W. H.; Sigg, L. Dynamic speciation analysis and bioavailability of metals in aquatic systems. *Environ. Sci. Technol.* **2005**, *39*, 8545-8556.

(103) Davison, W.; Zhang, H. Progress in understanding the use of diffusive gradients in thin films (DGT) – back to basics. *Environ. Chem.* **2012**, *9*, 1-13.

(104) Town, R. M.; Emons, H.; Buffle, J. Speciation analysis by electrochemical methods. In: *Handbook of Elemental Speciation: Techniques and Methodology*. R. Cornelis, H. Crews, J. Caruso, H. Heumann (Eds.), Wiley, Chapter 5.9, 2003, pp. 428-461.

(105) Morel, F. M. M.; Morel-Laurens, N. M. L. Trace metals and plankton in the oceans: facts and speculation. In: *Trace Metals in Sea Water*, Vol. 9, NATO conference Series 1983, pp. 841-869.

(106) van Leeuwen, H. P. Metal speciation dynamics and bioavailability: inert and labile complexes. *Environ. Sci. Technol.* **1999**, *33*, 3743-3748.

(107) van Leeuwen, H. P. Speciation dynamics and bioavailability of metals. *J. Radioanal. Nucl. Chem.* **2000**, *246*, 487-492.

(108) Duval, J; F. L. Dynamics of metal uptake by charged biointerphases: bioavailability and bulk depletion. *Phys. Chem. Chem. Phys.* **2013**, *15*, 7873-7888.

(109) Duval, J. F. L.; Rotureau, E. Dynamics of metal uptake by charged soft biointerphases: impacts of depletion, internalisation, adsorption and excretion. *Phys. Chem. Chem. Phys.* **2014**, *16*, 7401-7416.

(110) Duval, J. F. L.; Paquet, N.; Lavoie, M.; Fortin, C. Dynamics of metal partitioning at the cell-solution interface: Implications for toxicity assessment under growth inhibition conditions. *Environ. Sci. Technol.* **2015**, *49*, 6625-6636.

(111) Duval, J. F. L.; Présent, R. M.; Rotureau, E. Kinetic and thermodynamic determinants of trace metal partitioning at biointerphases: the role of intracellular speciation dynamics. *Phys. Chem. Chem. Phys.* **2016**, *18*, 30415-30435.

(112) Wilkinson, K. J.; Buffle, J. Critical evaluation of physicochemical parameters and processes for modelling the biological uptake of trace metals in environmental (aquatic systems). In *Physicochemical Kinetics and Transport at Biointerfaces*, IUPAC Series on Analytical and Physical Chemistry of Environmental Systems, Volume 9; van Leeuwen, H. P.; Köster, W., Eds.; Wiley: Chichester, 2004; pp 445-533.

(113) Campbell, P. G. C. Interactions between trace metals and aquatic organisms: a critique of the free-ion activity model. In *Metal Speciation and Bioavailability in Aquatic Systems*, IUPAC Series on Analytical and Physical Chemistry of Environmental Systems, Volume 3; Tessier, A.; Turner, D. R., Eds.; Wiley: Chichester, 1995; pp 45-102.

(114) Hudson, R. J. M. Which aqueous species control the rates of trace metal uptake by aquatic biota? Observations and predictions of nonequilibrium effects. *Sci. Total Environ.* **1998**, *219*, 95-115.

(115) van Ginneken, L.; Chowdhury, M. J.; Blust, R. Bioavailability of cadmium and zinc to common carp, *Cyprinus carpio*, in complexing environments: a test for the validity of the free ion activity model. *Environ. Toxicol. Chem.* **1999**, *18*, 2295-2304.

(116) Jansen, S.; Blust, R.; van Leeuwen, H. P. Metal speciation dynamics and bioavailability: Zn(II) and Cd(II) uptake by mussel (*Mytilus edulis*) and carp (*Cyprinus carpio*). *Environ. Sci. Technol.* **2002**, *32*, 2164-2170.

(117) Degryse, F.; Smolders, E.; Merckx, R. Labile Cd complexes increase Cd availability to plants. *Environ. Sci. Technol.* **2006**, *40*, 830-836.

(118) Bradac, P.; Behra, R.; Sigg, L. Accumulation of cadmium in periphyton under various freshwater speciation conditions. *Environ. Sci. Technol.* **2009**, *43*, 7291-7296.

(119) Ytreberg, E.; Karlsson, J.; Hoppe, S.; Eklund, B.; Ndungu, K. Effect of organic complexation on copper accumulation and toxicity to the estuarine red macroalga *Ceramium tenuicorne*: a test of the free ion activity model. *Environ. Sci. Technol.* **2011**, *45*, 3145-3153.

(120) Fortin, C.; Campbell, P. G. C. Silver uptake by the green alga, *Chlamydomonas reinhardtii*, in relation to chemical speciation: influence of chloride. *Environ. Toxicol. Chem.* **2000**, *19*, 2769-2778.

(121) Tipping, E.; Lofts, S. Testing WHAM-F_{TOX} with laboratory toxicity data for mixtures of metals (Cu, Zn, Cd, Ag, Pb). *Environ. Toxicol. Chem.* **2015**, *34*, 788-798.

(122) He, E.; van Gestel, C. A. M. Delineating the dynamic uptake and toxicity of Ni and Co mixtures in *Enchytraeus crypticus* using a WHAM-F_{TOX} approach. *Chemosphere* **2015**, *139*, 216-222.

(123) Bai, H.; Wei, S.; Jiang, Z.; He, M.; Ye, B.; Liu, G. Pb(II) bioavailability to algae (*Chlorella pyrenoidosa*) in relation to its complexation with humic acids of different molecular weight. *Ecotoxicol. Environ. Safety* **2019**, *167*, 1-9.

(124) De Schamphelaere, K. A. C.; Nys, C.; Janssen, C. R. Toxicity of lead (Pb) to freshwater green algae: development and validation of a bioavailability model and inter-species sensitivity comparison. *Aquat. Toxicol.* **2014**, *155*, 348-359.

(125) Sierra, J.; Roig, N.; Papiol, G. G.; Pérez-Gallego, E.; Schuhmacher, M. Prediction of the availability of potentially toxic elements in freshwaters. Comparison between speciation models and passive samplers. *Sci. Total Environ.* **2017**, *605-606*, 211-218.

(126) Constantino, C.; Scrimshaw, M.; Comber, S.; Churchley, J. An evaluation of biotic ligand models predicting acute copper toxicity to *Daphnia magna* in wastewater effluent. *Environ. Toxicol. Chem.* **2011**, *30*, 852-860.

(127) Prokop, Z.; Cupr, P.; Zlevorova-Zlamalikova, V.; Komarek, J.; Dusek, L.; Holoubek, I. Mobility, bioavailability, and toxic effects of cadmium in soil samples. *Environ. Res.* **2003**, *91*, 119-126.

(128) De Schamphelaere, K. A. C.; Heijerick, D. G.; Janssen, C. R. Refinement and field validation of a biotic ligand model predicting acute copper toxicity to *Daphnia magna*. *Comp. Biochem. Physiol. C: Toxicol. Pharmacol.* **2002**, *133*, 243-258.

(129) Qiu, H.; Versieren, L.; Rangel, G. G.; Smolders, E. Interactions and toxicity of Cu-Zn mixtures to *Hordeum vulgare* in different soils can be rationalized with bioavailability-based prediction models. *Environ. Sci. Technol.* **2016**, *50*, 1014-1022.

(130) Qiu, H.; Vijver, M. G.; He, E.; Liu, Y.; Wang, P.; Xia, B.; Smolders, E.; Versieren, L.; Peijnenburg, W. J. G. M. Incorporating bioavailability into toxicity assessment of Cu-Ni, Cu-Cd, and Ni-Cd mixtures with the extended biotic ligand model and the WHAM-F_{tox} approach. *Environ. Sci. Pollut. Res.* **2015**, *22*, 19213-19223.

(131) Stockdale, A.; Tipping, E.; Fjellheim, A.; Garmo, Ø. A.; Hildrew, A. G.; Lofts, A.; Monteith, D. T.; Ormerod, S. J.; Shilland, E. M. Recovery of macroinvertebrate species richness in acidified upland waters assessed with a field toxicity model. *Ecol. Indic.* **2014**, *37*, 341-350.

(132) Duval, J. F. L.; Town, R. M.; van Leeuwen, H. P. Applicability of the reaction layer principle to nanoparticulate metal complexes at a macroscopic reactive (bio)interface: a theoretical study. *J. Phys. Chem. C* **2017**, *121*, 19147-19161.

(133) Duval, J. F. L.; Town, R. M.; van Leeuwen, H. P. Lability of nanoparticulate metal complexes at a macroscopic metal responsive (bio)interface: expression and asymptotic scaling laws. *J. Phys. Chem. C* **2018**, *122*, 6052-6065.

(134) Eigen, M. Fast elementary steps in chemical reaction mechanisms. *Pure Appl. Chem.* **1963**, *6*, 97-115.

(135) van Leeuwen, H. P.; Town, R. M.; Buffle, J. Chemodynamics of soft nanoparticulate metal complexes in aqueous media. Basic theory for spherical particles with homogeneous spatial distributions of sites and charges. *Langmuir* **2011**, *27* 4514-4519.

(136) van Leeuwen, H. P. Eigen kinetics in surface complexation of aqueous metal ions. *Langmuir* **2008**, *24*, 11718-11721.

(137) Town, R. M.; Duval, J. F. L; Buffle, J.; van Leeuwen, H. P. Chemodynamics of metal complexation by natural soft colloids: Cu(II) binding by humic acid. *J. Phys. Chem. A* **2012**, *116*, 6489-6496.

(138) Buck, R. P. Diffuse layer charge relaxation at the ideally polarized electrode. *J. Electroanal. Chem.* **1969**, *23*, 219-240.

(139) van Leeuwen, H. P.; Buffle, J.; Town, R. M. Electric relaxation processes in chemodynamics of aqueous metal complexes: from simple ligand to soft nanoparticulate complexes. *Langmuir* **2012**, *28*, 227-234.

(140) Meylan, S.; Odzak, N.; Behra, R.; Sigg, L. Speciation of copper and zinc in natural freshwater: comparison of voltammetric measurements, diffusive gradients in thin films (DGT) and chemical equilibrium models. *Anal. Chim. Acta* **2004**, *510*, 91-100.

(141) Unsworth, E. R.; Warnken, K. W.; Zhang, H.; Davison, W.; Black, F.; Buffle, J.; Cao, J.; Cleven, R.; Galceran, J.; Gunkel, P.; Kalis, E.; Kistler, D.; van Leeuwen, H. P.; Martin, M.; Noël, S.; Nur, Y.; Odzak, N.; Puy, J.; van Riemsdijk, W.; Sigg, L.; Temminghoff, E.; Tercier-Waeber, M.-L.; Toepperwien, S.; Town, R. M.; Weng, L.; Xue, H. Model predictions of metal speciation in freshwaters compared to measurements by in situ techniques. *Environ. Sci. Technol.* **2006**, *40*, 1942-1949.

(142) Fortin, C.; Couillard, Y.; Vigneault, B.; Campbell, P. G. C. Determination of free Cd, Cu and Zn concentrations in lake waters by in situ diffusion followed by column equilibration ion-exchange. *Aquat. Geochem.* **2010**, *16*, 151-172.

(143) Ahmed, I. A. M.; Hamilton-Taylor, J.; Bieroza, M.; Zhang, H.; Davison, W. Improving and testing geochemical speciation predictions of metal ions in natural waters. *Wat. Res.* **2014**, *67*, 276-291.

(144) Balistrieri, L. S.; Blank, R. G. Dissolved and labile concentrations of Cd, Cu, Pb, and Zn in the South Fork Coeur d'Alene River, Idaho: comparisons among chemical equilibrium models and implications for biotic ligand models. *Appl. Geochem.* **2008**, *23*, 3355-3371.

(145) Unsworth, E. R.; Zhang, H.; Davison, W. Use of diffusive gradients in thin films to measure cadmium speciation in solutions with synthetic and natural ligands: comparison with model predictions. *Environ. Sci. Technol.* **2005**, *39*, 624-630.

(146) Domingos, R. F.; Benedetti, M. F.; Croué, J. P.; Pinheiro, J. P. Electrochemical methodology to study labile trace metal/natural organic matter complexation at low concentration levels in natural waters. *Anal. Chim. Acta* **2004**, *521*, 77-86.

(147) Meylan, S.; Odzak, N.; Behra, R.; Sigg, L. Speciation of copper and zinc in natural freshwater: comparison of voltammetric measurements, diffusive gradients in thin films (DGT) and chemical equilibrium models. *Anal. Chim. Acta* **2004**, *510*, 91-100.

(148) Peng, L.; Shi, Z.; Wang, P.; Li, W.; Lin, Z.; Dang, Z.; Sparks, D. L. A novel multi-reaction model for kinetics of Zn release from soils: roles of soil binding sites. *J. Coll. Interf. Sci.* **2018**, *514*, 146-155.

(149) Warnken, K. W.; Lawlor, A. J.; Lofts, S.; Tipping, E.; Davison, W.; Zhang, H. In situ speciation measurements of trace metals in headwater streams. *Environ. Sci. Technol.* **2009**, *43*, 7230-7236.

(150) Guthrie, J. W.; Hassan, N. M.; Salam, M. S. A.; Fasfous, I. I.; Murimboh, C. A.; Murimboh, J.; Chakrabarti, C. L.; Grégoire, D. C. Complexation of Ni, Cu, Zn, and Cd by DOC in some metal-impacted freshwater lakes: a comparison of approaches using electrochemical determination of free-metal-ion and labile complexes and a computer speciation model, WHAM V and VI. *Anal. Chim. Acta* **2005**, *528*, 205-218.

(151) Shi, Z.; Wang, P.; Peng, L.; Lin, Z.; Dang, Z. Kinetics of heavy metal dissociation from natural organic matter: roles of the carboxylic and phenolic sites. *Environ. Sci. Technol.* **2016**, *50*, 10476-10484.

(152) Wang, P.; Ding, Y.; Liu, M.; Liang, Y.; Shi, Z. Modeling kinetics of Ni dissociation from humic substances based on WHAM 7. *Chemosphere* **2019**, *221*, 254-262.

(153) Peng, L.; Liu, P.; Feng, X.; Wang, Z.; Cheng, T.; Liang, Y.; Lin, Z.; Shi, Z. Kinetics of heavy metal adsorption and desorption in soil: development of a unified model based on chemical speciation. *Geochim. Cosmochim. Acta* **2018**, *224*, 282-300.

TABLE OF CONTENTS ART